The tetraspanin Tspan15 is an essential subunit of an ADAM10 scissor complex

Chek Ziu Koo, Neale Harrison, Peter John Noy, Justyna Szyroka, Alexandra L Matthews, Hung-En Hsia, Stephan A Müller, Johanna Tüshaus, Joelle Goulding, Katie Willis, et al.

The tetraspanin Tspan15 is an essential subunit of an ADAM10 scissor complex

Received for publication, January 9, 2020, and in revised form, February 14, 2020 Published, Papers in Press, February 28, 2020, DOI 10.1074/jbc.RA120.012601

Chek Ziu Koo[‡§1], Neale Harrison[‡1], Peter J. Noy[‡1], Justyna Szyroka[‡], Alexandra L. Matthews[‡], Hung-En Hsia[¶], Stephan A. Müller[¶], Johanna Tüshaus[¶], Joelle Goulding[§‖], Katie Willis[‡], Clara Apicella[‡], Bethany Cragoe[‡], Edward Davis[‡], Murat Keles[‡], Antonia Malinova[‡], Thomas A. McFarlane[‡], Philip R. Morrison[‡], Hanh T. H. Nguyen[‡], Michael C. Sykes[‡], Haroon Ahmed[‡], Alessandro Di Maio[‡], Lisa Seipold[**], Paul Saftig[**], Eleanor Cull[‡], Christos Pliotas[‡‡], Eric Rubinstein[§§], Natalie S. Poulter[§¶¶], Stephen J. Briddon[§‖], Nicholas D. Holliday[‖], Stefan F. Lichtenthaler[¶], and Michael G. Tomlinson[‡§2]

From the [‡]School of Biosciences and the [¶¶]Institute of Cardiovascular Sciences, University of Birmingham, Birmingham B15 2TT, United Kingdom, the [§]Centre of Membrane Proteins and Receptors (COMPARE), Universities of Birmingham and Nottingham, Midlands B15 2TT, United Kingdom, the [¶]German Center for Neurodegenerative Diseases (DZNE) Munich, Neuroproteomics, Klinikum rechts der Isar, Technical University Munich and Munich Cluster for Systems Neurology (SyNergy), 81377 Munich, Germany, the [‖]Division of Physiology, Pharmacology and Neuroscience, School of Life Sciences, University of Nottingham, Nottingham NG7 2UH, United Kingdom, the [**]Institute of Biochemistry, Christian Albrechts University Kiel, 24118 Kiel, Germany, the [‡‡]School of Biomedical Sciences, Faculty of Biological Sciences, University of Leeds, Leeds LS2 9JT, United Kingdom, and [§§]Sorbonne Université, INSERM, CNRS, Centre d'Immunologie et des Maladies Infectieuses, CIMI-Paris, Paris 75013, France

Edited by Peter Cresswell

A disintegrin and metalloprotease 10 (ADAM10) is a transmembrane protein essential for embryonic development, and its dysregulation underlies disorders such as cancer, Alzheimer's disease, and inflammation. ADAM10 is a "molecular scissor" that proteolytically cleaves the extracellular region from >100 substrates, including Notch, amyloid precursor protein, cadherins, growth factors, and chemokines. ADAM10 has been recently proposed to function as six distinct scissors with different substrates, depending on its association with one of six regulatory tetraspanins, termed TspanC8s. However, it remains unclear to what degree ADAM10 function critically depends on a TspanC8 partner, and a lack of monoclonal antibodies specific for most TspanC8s has hindered investigation of this question. To address this knowledge gap, here we designed an immunogen to generate the first monoclonal antibodies targeting Tspan15, a model TspanC8. The immunogen was created in an ADAM10-knockout mouse cell line stably overexpressing human Tspan15, because we hypothesized that expression in this cell line would expose epitopes that are normally blocked by ADAM10. Following immunization of mice, this immunogen strategy generated four Tspan15 antibodies. Using these antibodies, we show that endogenous Tspan15 and ADAM10 co-localize on the cell surface, that ADAM10 is the principal Tspan15-interacting protein, that endogenous Tspan15 expression requires ADAM10 in cell lines and primary cells, and that a synthetic ADAM10/Tspan15 fusion protein is a functional scissor. Furthermore, two of the four antibodies impaired ADAM10/Tspan15 activity. These findings suggest that Tspan15 directly interacts with ADAM10 in a functional scissor complex.

A disintegrin and metalloproteinase 10 (ADAM10)[3] is a ubiquitously expressed transmembrane protein that acts as a "molecular scissor" by cleaving the extracellular region from over 100 substrates, a process termed ectodomain shedding (1). ADAM10 is essential for embryonic development by activating Notch proteins, which determine cell fate. Other substrates include cadherin adhesion molecules, amyloid precursor protein, and transmembrane growth factors and chemokines. As such, ADAM10 is important for health and in diseases such as cancer, Alzheimer's, and inflammatory diseases (2).

The tetraspanins are a superfamily of 33 transmembrane proteins in mammals, which interact with specific transmembrane partner proteins and regulate their intracellular trafficking, lateral mobility, and clustering at the cell surface (3, 4). The

This work was funded by a British Heart Foundation Ph.D. Studentship Grant FS/18/9/33388 and COMPARE (to C. Z. K.), Biotechnology and Biological Sciences Research Council Project Grant BB/P00783X/1 (to N. H.), British Heart Foundation Project Grant PG/13/92/30587 (to P. J. N.), Biotechnology and Biological Sciences Research Council Ph.D. Studentships (to J. S. and A. L. M.), and a Biochemical Society Summer Vacation Studentship (to H. T. H. N.). This work was also supported by the Deutsche Forschungsgemeinschaft (German Research Foundation) within the framework of the Munich Cluster for Systems Neurology (EXC 2145 SyNergy, project ID 390857198) and by the BMBF through CLINSPECT-M (to S. F. L.). Further support was provided by Deutsche Forschungsgemeinschaft Grant DFG-SFB877-A3 (to P. S.). The authors declare that they have no conflicts of interest with the contents of this article.

This article contains Table S1 and Figs. S1–S3.

[1] These authors contributed equally to this work.

[2] To whom correspondence should be addressed: School of Biosciences, College of Life and Environmental Sciences, University of Birmingham, Birmingham B15 2TT, United Kingdom. Tel.: 44-121-414-2507; Fax: 44-121-414-5925; E-mail: m.g.tomlinson@bham.ac.uk.

[3] The abbreviations used are: ADAM10, a disintegrin and metalloprotease 10; DAPT, *N*-[*N*-(3,5-difluorophenacetyl)-L-alanyl]-*S*-phenylglycine *t*-butyl ester; LEL, large extracellular loop; MEF, mouse embryonic fibroblast; NEM, *N*-ethylmaleimide; TIRF, total internal reflection fluorescence; ER, endoplasmic reticulum; HUVEC, human umbilical vein endothelial cell; qRT-PCR, quantitative RT-PCR; BiFC, bimolecular fluorescence complementation; sfGFP, superfolder GFP; FCS, fluorescence correlation spectroscopy; PCH, photon-counting histogram; KO, knockout; BTRC, β-transducin repeat–containing E3 ubiquitin protein ligase; GAPDH, glyceraldehyde-3-phosphate dehydrogenase; ANOVA, analysis of variance.

first crystal structure of a tetraspanin suggests the capacity for conformational change, regulated by cholesterol binding within a cavity formed by the four transmembrane helices (5). This raises the possibility that tetraspanins regulate their partner proteins as molecular switches. We and others have identified six TspanC8 tetraspanins as regulators of ADAM10 intracellular trafficking and enzymatic maturation (6–8). The TspanC8s comprise Tspan5, -10, -14, -15, -17, and -33 and are so-called because of eight cysteines within their large extracellular loop. Different cell types express distinct TspanC8 repertoires (9, 10), and emerging evidence suggests that each TspanC8 may cause ADAM10 to cleave specific substrates (6, 11–16). However, there is an urgent need to generate mAbs to all TspanC8s, to define fully their expression profiles and functional mechanisms. Moreover, it remains to be determined whether ADAM10 functions as an intimate ADAM10/TspanC8 complex or whether TspanC8s are merely modulators of ADAM10 trafficking.

This study focuses on Tspan15 as a model TspanC8. Human Protein Atlas mRNA data indicate that Tspan15 is expressed within most tissue types, but only by approximately one-third of cancer cell lines, and not by most blood cell types (17, 18). Tspan15 is best-characterized by its capacity to promote ADAM10 cleavage of N-cadherin in cell lines and *in vivo* (8, 12, 13, 16). Tspan15 is also up-regulated and is a marker of poor prognosis in certain cancers (19–21), and it promotes cancer progression in a mouse model (21).

The aims of this study were 2-fold: first, to develop a novel strategy for tetraspanin mAb generation to make and characterize the first Tspan15 mAbs, and second, to use these mAbs to test four hypotheses that would support the theory that Tspan15 and ADAM10 exist together as a scissor complex: 1) that endogenous Tspan15 and ADAM10 co-localize on the cell surface; 2) that ADAM10 is the principal Tspan15-interacting protein; 3) that Tspan15 expression requires ADAM10; and 4) that covalently linking Tspan15 and ADAM10 together as a single fusion protein yields a functional scissor.

Results

Generation of Tspan15 mAbs using a novel immunogen strategy

The majority of anti-tetraspanin mAbs have epitopes within the large extracellular loop (LEL). However, it has been traditionally difficult to make mAbs to many tetraspanins due to lack of efficacy of recombinant LELs as immunogens. Furthermore, use of tetraspanins expressed in whole cells as the immunogen is complicated by their relatively high sequence conservation between species, their relatively small size, and possible masking of mAb epitopes by larger partner proteins (22). We therefore hypothesized that expression of human Tspan15 in ADAM10-knockout mouse cells would "unmask" Tspan15, allowing the generation of a mAb response in mice immunized with these cells. Thus, ADAM10-knockout mouse embryonic fibroblasts (MEFs) (23) stably overexpressing FLAG-tagged human Tspan15 were generated by lentiviral transduction, and cell lysates (generated using the widely used 1% Triton X-100 lysis buffer) were immunoblotted with a FLAG antibody to confirm expression (Fig. 1*A*). Immunization of mice with these cells, and subsequent hybridoma generation, was outsourced to Abpro Therapeutics. Four positive hybridomas were identified by screening of hybridoma tissue culture supernatants by flow cytometry of WT *versus* CRISPR/Cas9 Tspan15-knockout Jurkat T cells (Fig. 1*B*). The mAbs were isotyped as IgG1κ for clones 1C12, 4A4, and 5D4 and as IgG2Bκ for 5F4 (data not shown). To investigate whether the Tspan15 mAbs might cross-react with other members of the TspanC8 family, human embryonic kidney (HEK)-293T cells were transfected with FLAG-tagged Tspan5, Tspan10, Tspan14, Tspan15, Tspan17, or Tspan33, and whole-cell lysates were Western blotted. Tspan15 was detected by each of the four Tspan15 mAbs, but none of the other TspanC8s were detected (Fig. 1*C*). To determine whether the Tspan15 mAbs can co-immunoprecipitate ADAM10, human platelets were lysed in the relatively stringent 1% digitonin lysis buffer that was previously used to identify TspanC8/ADAM10 interactions (6, 7). Tspan15 immunoprecipitation followed by ADAM10 Western blotting showed that each mAb effectively co-immunoprecipitated ADAM10 (Fig. 1*D*). Therefore, these data validate the four new mAbs as specific mouse anti-human Tspan15 reagents capable of immunoprecipitating Tspan15/ADAM10 complexes.

To determine whether our novel immunogen strategy may be useful for other tetraspanins, the same strategy was used for Tspan14, another member of the TspanC8 subgroup. This generated five mouse anti-human Tspan14 monoclonal antibodies, which were selected by flow cytometry screening of HEK-293T cells transiently overexpressing Tspan14 (Fig. S1). However, these mAbs did not detect overexpressed Tspan14 by Western blotting and did not detect endogenous Tspan14 by flow cytometry in several cell lines tested (data not shown); the selected antibodies may be low-affinity. Nevertheless, this suggests that mouse cell lines engineered to lack a tetraspanin partner are promising immunogens for the generation of antibody responses in mice to the human tetraspanin.

The four Tspan15 mAbs bind to similar epitopes in the large extracellular loop

To determine whether the Tspan15 mAbs have epitopes in the LEL, previously described Tspan15/Tspan5 chimeric GFP-tagged constructs were used in which the LELs were exchanged (15). In flow cytometry analyses of transfected HEK-293T cells, the four Tspan15 mAbs detected the Tspan15 LEL on a Tspan5 backbone (*T5-LEL15*), but not the reciprocal protein (*T15-LEL5*) (Fig. 2*A*). As a control, a Tspan5 mAb detected Tspan5 LEL on a Tspan15 backbone (Fig. 2*A*), as reported previously (15). To investigate whether the Tspan15 mAbs have overlapping epitopes, an antibody-binding competition assay was performed. To do this, the A549 lung epithelial cell line was preincubated with one of the Tspan15 mAbs or a negative control antibody and then incubated with Tspan15 mAbs conjugated to Alexa Fluor® 647. Flow cytometry analyses showed that all four unlabeled Tspan15 mAbs inhibited binding of each of the four labeled Tspan15 mAbs (Fig. 2*B*), suggesting that their epitopes are located in close proximity. Within the Tspan15 LEL, only eight of the 121 amino acid residues vary between mice and humans, all within the C-terminal half of the LEL (Fig. 2*C*).

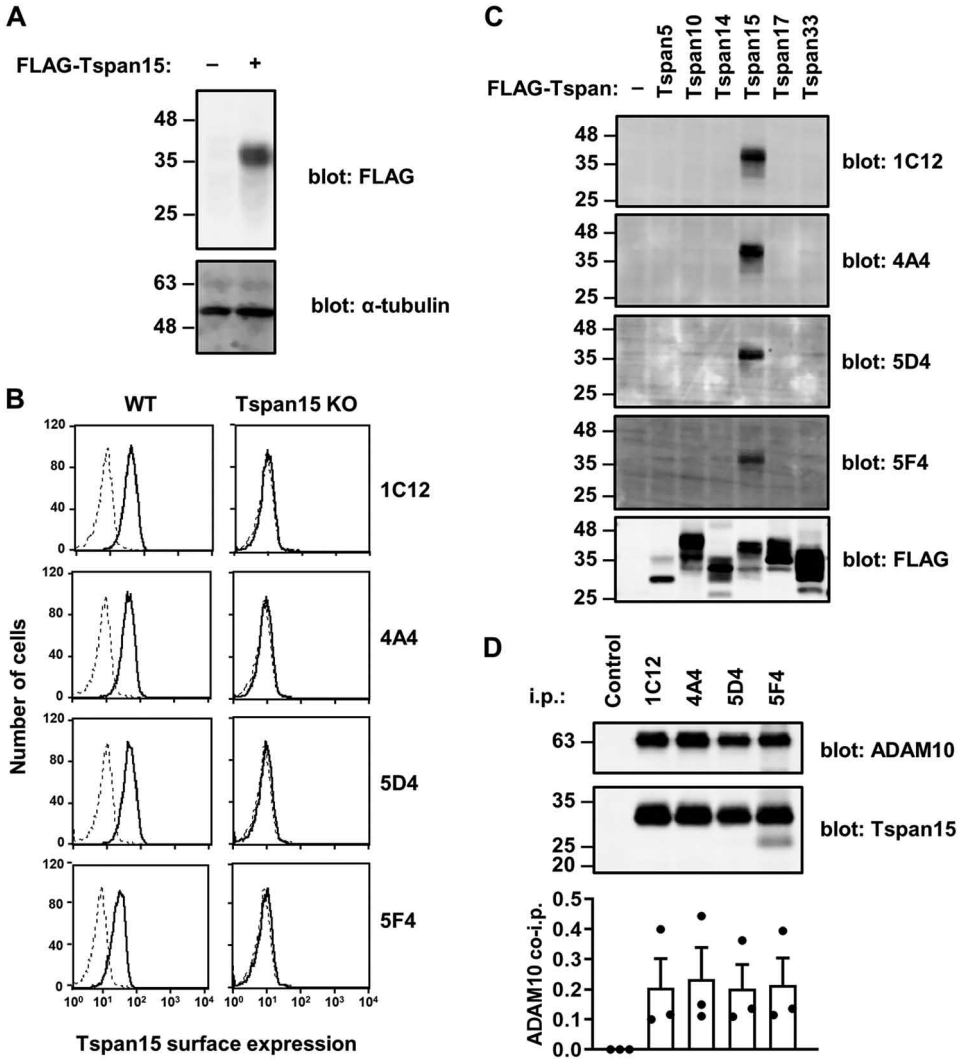

Figure 1. Generation of human Tspan15-expressing MEFs as an immunogen and validation of resulting mouse anti-human Tspan15 mAbs. *A*, ADAM10-knockout MEFs (−) and ADAM10-knockout MEFs stably overexpressing FLAG-tagged Tspan15 (+) were lysed in 1% Triton X-100 lysis buffer and subjected to anti-FLAG (*top*) and anti-α-tubulin (*bottom*) Western blotting. *B*, WT and Tspan15-KO Jurkat human T cells were analyzed by flow cytometry with tissue culture supernatant for each of the four mouse anti-human Tspan15 hybridomas (1C12, 4A4, 5D4, or 5F4; *solid line*) or with mouse IgG1 as a negative control (*dotted line*). Histograms are representative of two independent experiments. *C*, HEK-293T cells were transfected with FLAG-tagged human TspanC8 expression constructs (except for Tspan10, which was of mouse origin) or an empty vector control (−), lysed in 1% Triton X-100 lysis buffer and Western blotted with tissue culture supernatants for each of the four Tspan15 hybridomas, or a positive control FLAG antibody. Blots are representative of three independent experiments. *D*, human platelets were lysed in 1% digitonin lysis buffer and subjected to immunoprecipitation (*i.p.*) with the four Tspan15 mAbs or a negative control mouse IgG1, followed by anti-ADAM10 and anti-Tspan15 (5D4) Western blotting (*top panels*). The faint additional band in the *5F4 lane* corresponds to light chain from the immunoprecipitating mAb (data not shown). To quantitate the data, the amount of ADAM10 co-immunoprecipitated was normalized to the amount of immunoprecipitated Tspan15 with each antibody (*bottom*). *Error bars*, S.E. from three independent experiments.

Because none of the Tspan15 mAbs detected mouse Tspan15 by Western blotting (Fig. 2*D*), this suggested that some of the differing residues were important for antibody binding. To determine which were important, four FLAG-tagged Tspan15 human/mouse chimeric constructs were made by substituting residues within the LEL of human Tspan15 with the corresponding mouse residues (Fig. 2*C*), an approach that we used previously to epitope-map mAbs to tetraspanin CD53 (24, 25). Western blotting of lysates from transfected Tspan15-knockout HEK-293T cells showed that reactivity of all four Tspan15 mAbs was almost completely lost by changing residues FSV to LNA but was unaffected in the three other chimeras (Fig. 2*D*). However, the human FSV sequence was not sufficient for recognition, because introduction of these residues into mouse Tspan15 did not enable recognition by the four Tspan15 mAbs (Fig. 2*D*). To gain further insights into the antibody-binding region, a Tspan15 model structure was generated, based on the crystal structure of CD81 (5). This model suggested that the critical FSV sequence is close to the top of the Tspan15 molecule, adjacent to a predicted α helix in the variable region (Fig. 2*E*). Interestingly, the mAbs detected overexpressed mouse Tspan15 by flow cytometry, and clones 1C12 and 4A4 were more effective than 5D4 and 5F4 (Fig. S2). This contrasts with their complete lack of reactivity to mouse Tspan15 by Western blotting (Fig. 2*D*), but nevertheless demonstrates at least some affinity for the mouse protein. Taken together, these data identify the FSV sequence in the LEL as an important component of the epitope for all four mAbs, but there may be subtle differences in epitopes for each one.

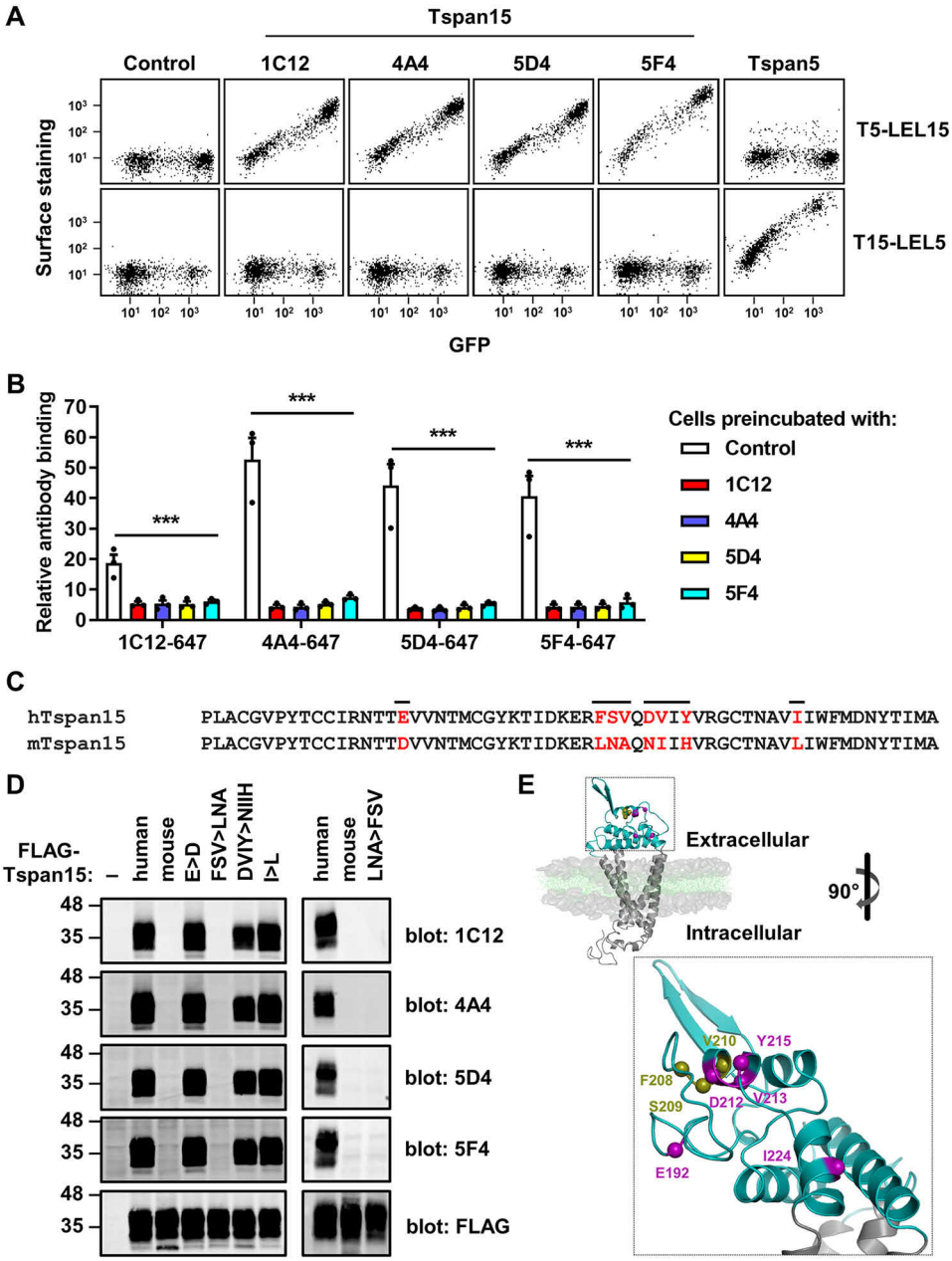

Figure 2. The four Tspan15 mAbs bind to similar epitopes in the large extracellular loop. *A*, Tspan15-knockout HEK-293T cells were transfected with GFP-tagged Tspan5 with the large extracellular loop of Tspan15 (*T5-LEL15*) or the reciprocal chimeric expression construct (*T15-LEL5*). Cells were stained with the four Tspan15 mAbs (1C12, 4A4, 5D4, or 5F4), Tspan5 mAb (TS5-2), or negative control mouse IgG1, followed by allophycocyanin-conjugated anti-mouse antibody and flow cytometry analyses. *B*, A549 cells were preincubated with one of the four unlabeled Tspan15 mAbs or MOPC-21 negative control mouse IgG1 for 30 min and stained with Alexa Fluor® 647–conjugated Tspan15 mAbs. Antibody binding, relative to unstained cells, was quantitated by flow cytometry. Data were log-transformed and statistically analyzed by a two-way ANOVA with Tukey's multiple-comparison test. *Error bars*, S.E. from three independent experiments (***, $p < 0.001$ for control compared with each of the mAb preincubations). *C*, amino acid sequence alignment of the C-terminal half of human (*h*) and mouse (*m*) Tspan15 large extracellular loop region with Clustal Omega (61). Sequence differences are shown in *red*, and sequences exchanged in the four mutant constructs are indicated by *horizontal lines above* the line-up. *D*, Tspan15-knockout HEK-293T cells were transfected with FLAG-tagged human Tspan15, mouse Tspan15, four chimeric constructs with human Tspan15 residues replaced by corresponding mouse residues, a chimeric construct comprising mouse Tspan15 with three residues of the corresponding human sequence, or an empty vector control (−). Cells were lysed in 1% Triton X-100 lysis buffer and subjected to anti-Tspan15 or anti-FLAG Western blotting. Data are representative of three experiments, from which quantitation demonstrated no significant detection of mouse Tspan15 or the FSV to LNA and reciprocal chimera (data not shown). *E*, predicted structure of human Tspan15, showing the location of epitopes recognized by Tspan15 mAbs (*olive*) and other residues that differ from mouse Tspan15 (*magenta*) in the extracellular region (*cyan*).

Tspan15 mAbs 1C12 and 4A4 impair Tspan15/ADAM10 activity

To test whether the four Tspan15 mAbs modulate Tspan15/ADAM10 activity, their effects on VE-cadherin cleavage were assessed in transfected HEK-293T cells. This assay was chosen because VE-cadherin cleavage was strikingly dependent on Tspan15 in this transfection system following ADAM10 activation with the alkylating agent *N*-ethylmaleimide (NEM) (Fig. 3*A*), even though we have previously reported no such dependence on Tspan15 for endogenous VE-cadherin in human umbilical vein endothelial cells (HUVECs) (14). Tspan15 mAbs 1C12 and 4A4 at 10 μg/ml inhibited VE-cadherin cleavage by

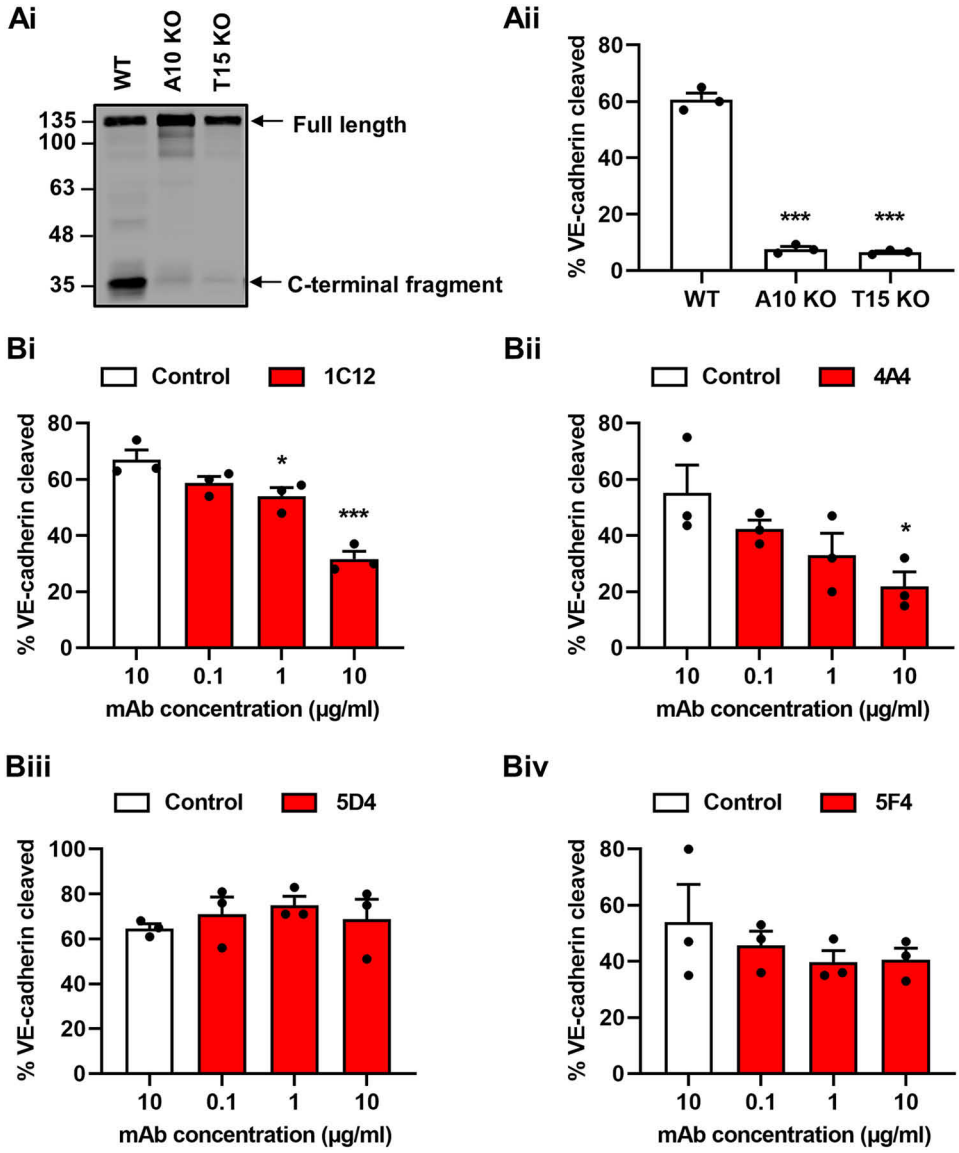

Figure 3. Tspan15 mAbs 1C12 and 4A4 partially inhibit ADAM10/Tspan15 activity. *Ai*, WT, ADAM10-knockout (*A10 KO*), and Tspan15-knockout (*T15 KO*) HEK-293T cells were transfected with a VE-cadherin expression construct. Cells were treated with 10 μM DAPT to prevent post-ADAM10 proteolysis by γ-secretase, followed by 2 mM NEM for 30 min to activate ADAM10. Cells were lysed in 1% Triton X-100 lysis buffer and subjected to Western blotting with an antibody against the cytoplasmic tail of VE-cadherin. No C-terminal fragment was detected in the absence of NEM (data not shown). *Aii*, VE-cadherin cleavage data were quantitated to calculate the percentage cleaved. Data were arcsine-transformed and statistically analyzed by a one-way ANOVA with a Dunnett's multiple-comparison test (***, $p < 0.001$ compared with WT). *Error bars*, S.E. from three independent experiments. *B*, WT HEK-293T cells were transfected with VE-cadherin, treated with Tspan15 mAbs or MOPC-21 negative control mAb for 30 min, and stimulated with NEM as described for *A*. The cleavage of VE-cadherin was detected by Western blotting and quantitated as described in *A* for mAbs 1C12 (*Bi*), 4A4 (*Bii*), 5D4 (*Biii*), and 5F4 (*Biv*). *Error bars*, S.E. from three independent experiments (*, $p < 0.05$; ***, $p < 0.001$ compared with controls).

~50%, and a titration effect was observed with lower concentrations (Fig. 3, *Bi* and *Bii*). In contrast, mAbs 5D4 and 5F4 had no effect (Fig. 3, *Biii* and *Biv*). The reason for the different effects of the mAbs is not known, but it could be related to subtle differences in epitope, given that 1C12 and 4A4 more efficiently detected mouse Tspan15 by flow cytometry (Fig. S2). Nevertheless, these data show that certain Tspan15 mAbs can inhibit ADAM10/Tspan15 activity.

Tspan15 and ADAM10 co-localize on the cell surface

Epitope-tagged Tspan15 is known to co-localize with ADAM10 in transfected cells (6, 8), but this has yet to be confirmed for endogenous proteins. To address this, endogenous Tspan15 and ADAM10 were visualized on the surface of A549 cells by total internal reflection fluorescence (TIRF) microscopy. Tspan15 showed substantial co-localization with ADAM10, in contrast to the non-TspanC8 tetraspanin CD9, which was used as a control (Fig. 4*Ai*). Quantitation of the imaging data using Manders' coefficient showed that significantly more of the Tspan15/ADAM10 overlapping signal was present within total ADAM10 signal compared to the proportion of CD9/ADAM10 overlapping signal within total ADAM10 signal (M1) (Fig. 4*Aii*). Consistent with this, significantly more of the Tspan15/ADAM10 signal was present within total Tspan15 signal than CD9/ADAM10 was within total CD9 signal (M2) (Fig. 4*Aii*). In addition, significantly more

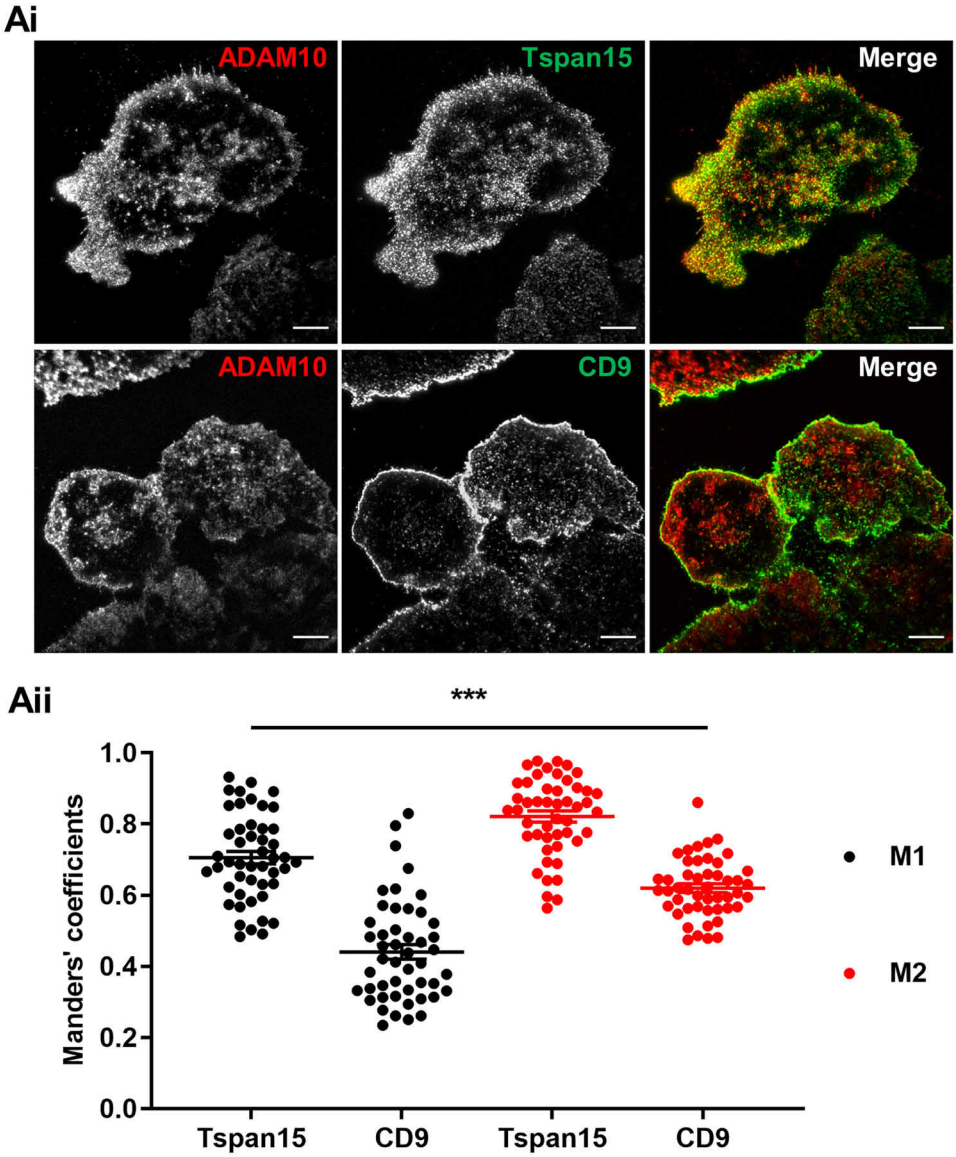

Figure 4. Tspan15 and ADAM10 co-localize on the cell surface. *Ai*, A549 cells were fixed and stained with anti-ADAM10 mAb (*red*) and either anti-Tspan15 mAb 5D4 (*green*) or anti-CD9 mAb 1AA2 (*green*). ADAM10, Tspan15, and CD9 on the basal membrane were imaged using TIRF microscopy. Images shown are representative of 48 fields of view from four independent experiments (*scale bar*, 10 μm). *Aii*, the degree of co-localization between ADAM10 and Tspan15 or CD9 was determined using Manders' coefficients to measure the proportion of overlapping pixels contained within total ADAM10 signal in the red channel (*M1*) and total Tspan15 or CD9 signal in the green channel (*M2*). Data were arcsine-transformed and statistically analyzed by a one-way ANOVA with Tukey's multiple-comparison test to compare M1 and M2, within and between Tspan15 and CD9 (***, $p < 0.001$ for all pairwise comparisons). *Error bars*, S.E.

of the Tspan15/ADAM10 overlapping signal was within total Tspan15 (M2), than was within total ADAM10 (M1) (Fig. 4*Aii*). This is consistent with the expression of other TspanC8s in A549 cells (7) that can form independent complexes with ADAM10.

ADAM10 is the principal Tspan15-interacting protein

The generation of Tspan15 mAbs enabled the first proteomic identification of interactors with endogenous Tspan15. To do this, Tspan15 mAb 1C12 was used to immunoprecipitate Tspan15 from WT HEK-293T cells lysed in the relatively stringent detergent 1% digitonin; Tspan15-knockout cells were used as a negative control. Subsequent MS identification revealed 27 proteins that were significantly detected in WT *versus* Tspan15-knockout samples from five independent experiments (Table 1 and Table S1). Expression of the entire data set as a volcano plot illustrated how the most significant and differential protein identified was ADAM10 (Fig. 5). Indeed, ADAM10 and Tspan15 were the only proteins above the false discovery threshold for these experiments (Fig. 5). These data suggest that ADAM10 is the principal Tspan15-interacting protein in HEK-293T cells.

Tspan15 protein expression requires ADAM10

It is well-established that TspanC8s promote the enzymatic maturation and trafficking of ADAM10 from the endoplasmic reticulum (ER) to the cell surface (6–8). More recently, it was suggested that the reverse might be true, because ADAM10 knockdown reduced the trafficking of Tspan5 from the ER in HCT116 and U2OS cell lines (15). To investigate whether

Table 1

Proteins identified in Tspan15 immunoprecipitates

The table contains proteins significantly enriched in the Tspan15 immunoprecipitation samples of WT compared with Tspan15-KO samples. Five additional proteins detected in WT samples (in at least three of five biological replicates), but not in more than one Tspan15 KO sample, are indicated with an asterisk. UniProt accession, protein name, gene name, *p* value, and -fold difference between WT and Tspan15 KO samples are listed. In addition, UniProt annotations indicate the localization of the proteins.

Accession	Protein name	Gene name	*p* value	-Fold difference (WT *vs.* KO)	Localization
O14672	A disintegrin and metalloproteinase domain-containing protein 10	*ADAM10*	1.70E − 08	397.32	Membrane
O95858	Tetraspanin-15	*TSPAN15*	3.38E − 05	18.57	Membrane
P62879	Guanine nucleotide-binding protein G(I)/G(S)/G(T) subunit β-2	*GNB2*	2.80E − 02	3.02	Cytoplasm
Q08380	Galectin-3-binding protein	*LGALS3BP*	2.92E − 03	2.92	
Q14315	Filamin-C	*FLNC*	1.10E − 02	2.34	Cytoplasm, membrane
P46779	60S ribosomal protein L28	*RPL28*	3.47E − 02	1.89	
P27824	Calnexin	*CANX*	1.82E − 02	1.86	Membrane
Q8WU90	Zinc finger CCCH domain-containing protein 15	*ZC3H15*	1.51E − 02	1.75	Cytoplasm
Q8NEZ5	F-box only protein 22	*FBXO22*	1.02E − 02	1.70	Cytoplasm
Q9HAD4	WD repeat-containing protein 41	*WDR41*	2.05E − 02	1.61	Cytoplasm
Q12907	Vesicular integral-membrane protein VIP36	*LMAN2*	1.97E − 02	1.59	Membrane
P63000	Ras-related C3 botulinum toxin substrate 1	*RAC1*	1.96E − 02	1.53	Cytoplasm, membrane
P23528	Cofilin-1	*CFL1*	3.95E − 02	1.45	Cytoplasm, membrane
Q4KMP7	TBC1 domain family member 10B	*TBC1D10B*	3.35E − 03	1.40	Cytoplasm
Q9Y2G5	GDP-fucose protein *O*-fucosyltransferase 2	*POFUT2*	3.52E − 02	1.35	
P36639	7,8-Dihydro-8-oxoguanine triphosphatase	*NUDT1*	2.69E − 02	1.35	Cytoplasm
Q15020	Squamous cell carcinoma antigen recognized by T-cells 3	*SART3*	4.79E − 02	1.34	Cytoplasm
Q9P2E9	Ribosome-binding protein 1	*RRBP1*	2.95E − 02	1.33	Membrane
Q13042	Cell division cycle protein 16 homolog	*CDC16*	2.39E − 02	1.31	Cytoplasm
P27348	14-3-3 protein θ	*YWHAQ*	2.66E − 02	1.27	Cytoplasm
Q8WUM4	Programmed cell death 6-interacting protein	*PDCD6IP*	1.56E − 02	1.24	Cytoplasm
P40926	Malate dehydrogenase, mitochondrial	*MDH2*	3.49E − 02	1.18	
P62304	Small nuclear ribonucleoprotein E	*SNRPE*	*	0.73	Cytoplasm
O43172	U4/U6 small nuclear ribonucleoprotein Prp4	*PRPF4*	*	1.45	
Q99878	Histone H2A type 1-J	*HIST1H2AJ*	*	0.73	
P51809	Vesicle-associated membrane protein 7	*VAMP7*	*	1.88	Membrane
Q7L576	Cytoplasmic FMR1-interacting protein 1	*CYFIP1*	*		Cytoplasm

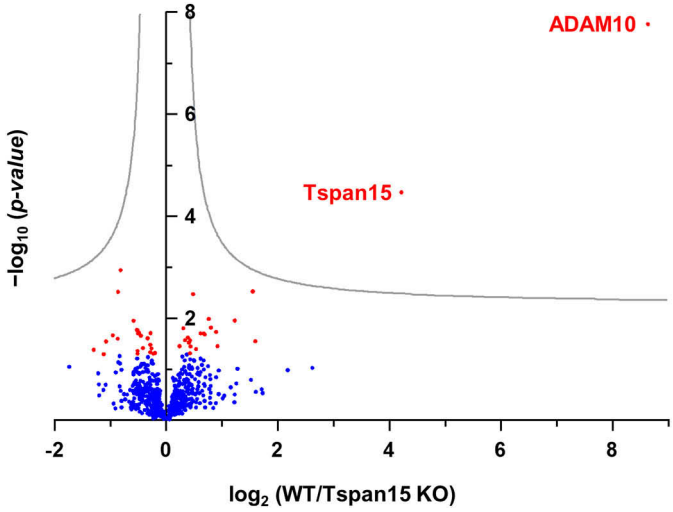

Figure 5. ADAM10 is the principal Tspan15-interacting protein in HEK-293T cells. WT and Tspan15-KO HEK-293T cells were lysed in 1% digitonin lysis buffer and immunoprecipitated with Tspan15 mAb 1C12 cross-linked to protein G–Sepharose beads. Proteins were identified by LC-MS/MS. Proteomic profiles of WT and Tspan15-KO HEK-293T immunoprecipitates are presented in a volcano plot to identify differentially expressed proteins. The minus $\log_{10}$-transformed *p* value of each protein was plotted against the $\log_2$-transformed protein label-free quantification ratio between the Tspan15 co-immunoprecipitation of WT samples and the control co-immunoprecipitation of Tspan15-KO samples. Proteins with significant -fold change ($p < 0.05$) are depicted in *red*; *blue dots* represent proteins with no significant changes in expression. A permutation-based false discovery rate estimation was applied and visualized as *hyperbolic curves* in *gray*.

Tspan15 surface expression also requires ADAM10, flow cytometry was performed on CRISPR/Cas9 ADAM10-knockout cell lines. Tspan15 surface expression, as revealed by flow cytometry, was reduced by ~80% in the absence of ADAM10 in Jurkat, HEK-293T, and A549 cells (Fig. 6*A*). This observation held true in primary cells, because Tspan15 expression was almost undetectable following siRNA knockdown of ADAM10 in human umbilical vein endothelial cells (HUVECs) (Fig. 6*B*). To determine whether the reduction in surface Tspan15 was consistent with a reduction in whole-cell Tspan15, Western blotting was performed on Tspan15 immunoprecipitates from Jurkat cell lysates. Similar to the flow cytometry data, Tspan15 protein expression was reduced by ~80% in the absence of ADAM10 (Fig. 6*C*). Importantly, the loss of Tspan15 protein was not a consequence of reduced Tspan15 mRNA expression in the absence of ADAM10, as this was unaffected in ADAM10-knockout cell lines as measured by quantitative RT-PCR (qRT-PCR) (Fig. 6*D*). To investigate the mechanism underlying the requirement of ADAM10 for Tspan15 expression, A549 cells were treated with the lysosomal inhibitor ammonium chloride. This significantly increased Tspan15 protein expression in ADAM10-knockout cells (Fig. 6*E*), whereas the proteasome inhibitor MG132 had no effect (data not shown). Interestingly, the molecular weight of Tspan15 was increased in ADAM10-knockout cells following lysosomal inhibition (Fig. 6*Ei*). This increase was due to aberrant glycosylation, because all Tspan15 bands on the blot were reduced to the same molecular weight following deglycosylation with peptide:*N*-glycosidase F (data not shown), indicating that ADAM10 affects Tspan15 glycosylation as has previously been reported for Tspan5 (15). Finally, lysosomal inhibition did not rescue cell surface expression of Tspan15 in the absence of ADAM10 (Fig. S3), indicating that an ADAM10/Tspan15 complex is required for trafficking to the cell surface. Together, these data demonstrate that ADAM10 and Tspan15 are each required for expression of the other, pro-

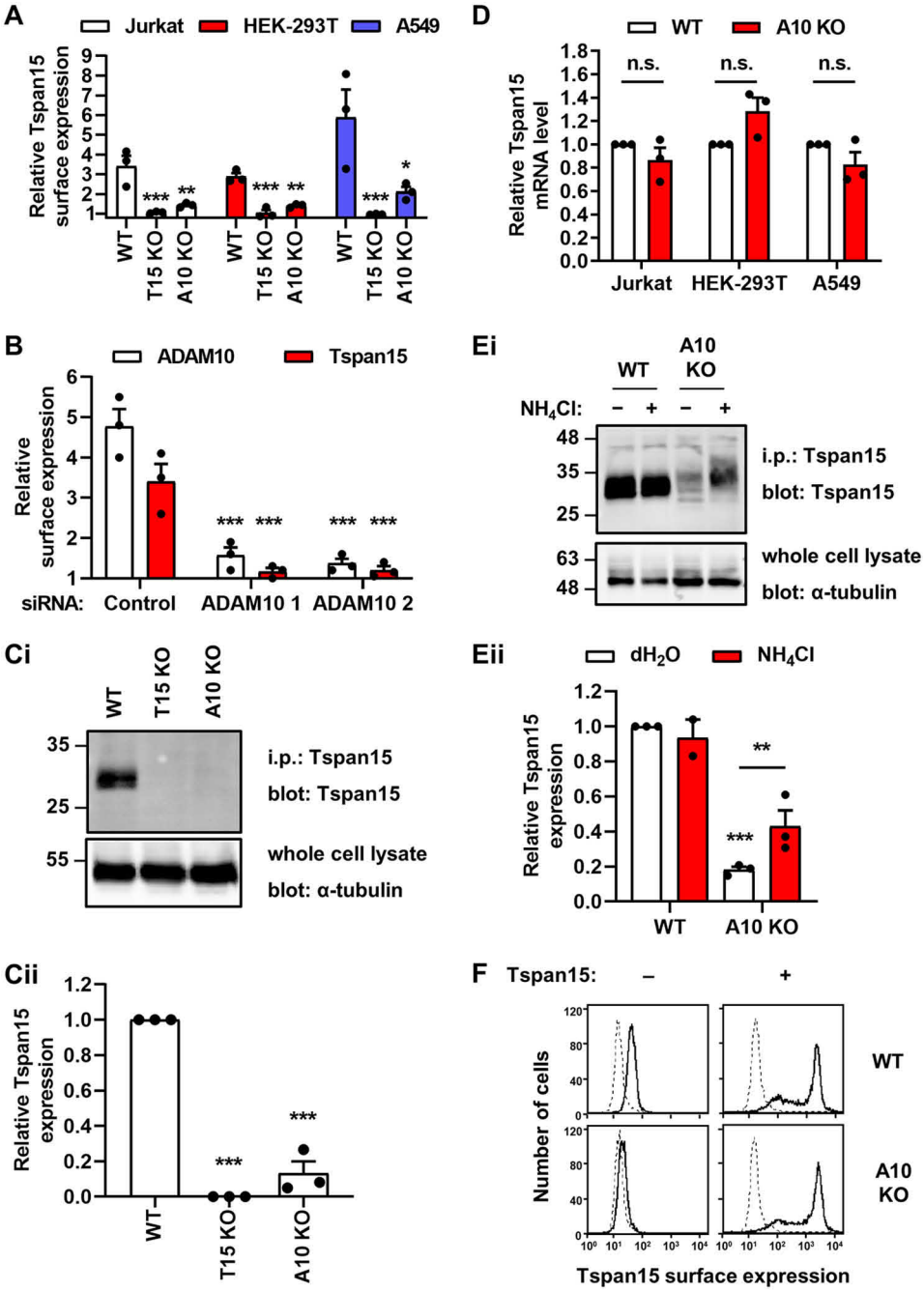

Figure 6. Tspan15 protein expression requires ADAM10. *A*, Tspan15 surface expression in WT, Tspan15-KO and ADAM10-KO Jurkat, HEK-293T, and A549 cell lines were analyzed by flow cytometry with anti-Tspan15 mAb 1C12 or mouse IgG1 negative control antibody. Tspan15 surface expression is presented as the geometric mean fluorescence intensity of Tspan15 staining relative to the control staining. *Error bars*, S.E. from three independent experiments. Data were log-transformed and statistically analyzed by a one-way ANOVA with Dunnett's multiple-comparison test (*, $p < 0.05$; **, $p < 0.01$; ***, $p < 0.001$ compared with WT). *B*, HUVECs were transfected with two different ADAM10 siRNAs or a negative control siRNA, and surface expression of ADAM10 and Tspan15 was measured by flow cytometry and analyzed as described in *A*. *Ci*, WT, Tspan15-KO and ADAM10-KO Jurkat cells were lysed in 1% Triton X-100 lysis buffer, immunoprecipitated with anti-Tspan15 mAb 5D4, and Western blotted with the same antibody. Whole-cell lysates were blotted with anti-α-tubulin mAb. *Cii*, Tspan15 levels from *Ci* were quantitated and normalized to WT expression. *Error bars*, S.E. from three independent experiments. Data were log-transformed and statistically analyzed by a one-way ANOVA with Tukey's multiple-comparison test (***, $p < 0.001$ compared with WT). *D*, Tspan15 mRNA level in WT and ADAM10-KO Jurkat, HEK-293T, and A549 cells were assessed by qRT-PCR and presented relative to GAPDH housekeeping gene expression. *Error bars*, S.E. from three independent experiments. Data were log-transformed and statistically analyzed by a two-way ANOVA followed by Tukey's multiple-comparison test (*n.s.*, not significant). *Ei*, WT and ADAM10-KO A549 cells were treated with 50 mM ammonium chloride lysosomal inhibitor or vehicle control for 20 h. Cells were lysed in 1% Triton X-100 lysis buffer, and Tspan15 immunoprecipitates and whole-cell lysates were Western blotted as described in *Ci*. *Eii*, Tspan15 levels from *Ei* were quantitated, normalized against tubulin levels, and presented relative to WT expression. Data were log-transformed and statistically analyzed by a two-way ANOVA with Tukey's multiple-comparison test (**, $p < 0.01$; ***, $p < 0.001$ compared with WT). *Error bars*, S.E. from three independent experiments, except for WT cells treated with ammonium chloride, which were from two experiments. *F*, WT and ADAM10-KO HEK-293T cells were transfected with empty vector control (−) or Tspan15 (+) expression constructs. Tspan15 surface expression was measured by flow cytometry as described in *A*. Histograms are representative of four independent experiments.

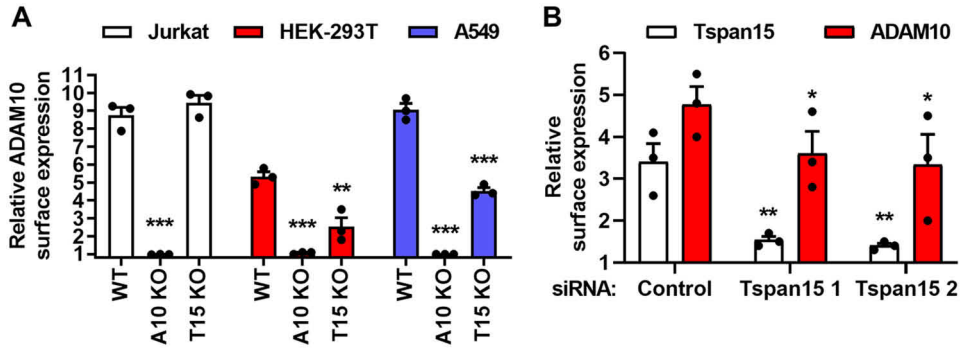

Figure 7. The requirement of Tspan15 for ADAM10 surface expression is cell type–dependent. *A*, ADAM10 surface expression in WT, ADAM10-KO and Tspan15-KO Jurkat, HEK-293T, and A549 cells was measured by flow cytometry and quantitated as described in Fig. 4*A*. *B*, HUVECs were transfected with two different Tspan15 siRNAs or negative control siRNA, and surface expression of ADAM10 was measured by flow cytometry and analyzed as described in Fig. 6*A*.

viding genetic evidence that the two proteins cooperate in a functional scissor complex.

The requirement of ADAM10 for normal Tspan15 protein expression is inconsistent with the fact that human Tspan15 was successfully expressed in ADAM10-knockout MEFs to generate the immunogen for Tspan15 mAb generation (Fig. 1*A*). To address whether overexpression of Tspan15 might overcome the requirement for ADAM10, HEK-293T cells were transiently transfected with Tspan15 and analyzed by flow cytometry. In this overexpression scenario, Tspan15 expression was comparable in WT *versus* ADAM10-knockout cells (Fig. 6*F*). Therefore, it appears that endogenous Tspan15 protein expression requires ADAM10, but overexpressed Tspan15 can bypass this requirement via a mechanism that remains unknown.

The requirement of Tspan15 for ADAM10 surface expression is cell type–dependent

To assess the extent to which Tspan15 is required for ADAM10 surface expression in the cells examined in Fig. 6, flow cytometry for ADAM10 was performed. ADAM10 surface expression was reduced by ~60 and 70% in Tspan15-knockout HEK-293T and A549 cells, respectively, but was unaffected in Jurkat T cells (Fig. 7*A*). In HUVECs, ADAM10 surface expression was reduced by ~40% following Tspan15 siRNA knockdown (Fig. 7*B*). Therefore, the importance of Tspan15 for ADAM10 surface expression depends on the cell type.

ADAM10 and Tspan15 form dynamic bimolecular fluorescence complementation (BiFC) complexes

A single-particle tracking study has previously reported an apparent diffusion coefficient for ADAM10 of 0.067 $\mu m^2/s$ in U2OS cells, which increased to 0.104 $\mu m^2/s$ following Tspan15 transfection (12). To more directly assess the lateral diffusion of ADAM10/Tspan15 complexes, and to image an ADAM10/Tspan15 dimer for the first time, BiFC was employed. This technique allows formation of fluorescent protein dimers from two interacting proteins tagged with split fluorescent proteins, in this case Tspan15 fused to the N-terminal half of superfolder GFP (sfGFP) and ADAM10 fused to the C-terminal half of sfGFP (Fig. 8*A*). Formation of fluorescent BiFC ADAM10/Tspan15 dimers was confirmed by confocal microscopy of transfected HEK-293T cells, which showed a BiFC signal predominantly at the cell surface, similar to Tspan15 itself (Fig. 8*B*). To examine the lateral diffusion of ADAM10/Tspan15 dimers on the apical membrane of transfected HEK-293T cells, fluorescence correlation spectroscopy (FCS) was used. The average number of fluorescent complexes/μm^2 was 48, and the average diffusion speed was 0.19 $\mu m^2/s$ (Fig. 8, *C* and *D*). To then provide an indication of the oligomerization state of the molecules, the average molecular brightness of ADAM10/Tspan15 dimers was determined using photon-counting histogram (PCH) analysis. Of the FCS traces analyzed, 58% fitted to a one-component PCH model (molecular brightness of 2.2×10^4 cpm/s), whereas the remaining preferentially fitted to a two-component model that had dimmer (1.4×10^4 cpm/s) and brighter (5.4×10^4 cpm/s) subcomponents (Fig. 8*E*). The molecular brightness of the dimmer traces was not significantly different from the one-component traces (Fig. 8*E*). The presence of a brighter subcomponent suggests that some ADAM10/Tspan15 complexes were able to form larger clusters. Collectively, these data show that ADAM10 and Tspan15 can interact with each other to form dynamic BiFC dimers of varying stoichiometric ratio within nanoclusters.

A synthetic ADAM10/Tspan15 fusion protein is a functional scissor

If ADAM10 and Tspan15 cooperate in a functional scissor complex, one prediction is that covalently linking the two proteins into one synthetic fusion protein (Fig. 9*A*) would not disrupt subcellular localization or scissor function. An ADAM10/Tspan15 fusion expression construct was generated and transfected into ADAM10/Tspan15 double-knockout HEK-293T cells. Western blotting with ADAM10 and Tspan15 mAbs verified that the ADAM10/Tspan15 fusion protein had the predicted molecular weight of ~95 kDa (Fig. 9*B*), and flow cytometry (Fig. 9*C*) and confocal microscopy (Fig. 9*D*) showed that it was expressed at the cell surface. To test scissor function, ADAM10/Tspan15 double-knockout HEK-293T cells were transfected with an expression construct for alkaline phosphatase–tagged betacellulin, a known ADAM10 substrate (26), and shedding was quantitated by measuring alkaline phosphatase activity released into the culture supernatant *versus* the nonshed activity remaining with the cells. Transfection of ADAM10/Tspan15 double-knockout cells with the ADAM10/Tspan15 fusion protein construct restored betacellulin shed-

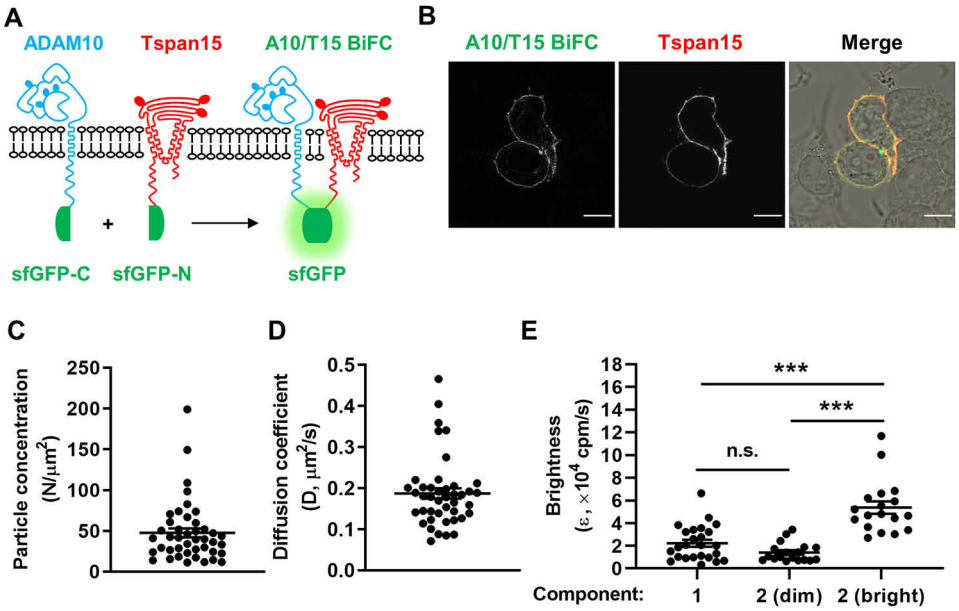

Figure 8. ADAM10 and Tspan15 form dynamic BiFC complexes. *A*, *schematic representation* of ADAM10 tagged with the C-terminal half of sfGFP (*sfGFP-C*), Tspan15 tagged with the N-terminal half of sfGFP (*sfGFP-N*), and the predicted ADAM10/Tspan15 BiFC dimer. *Solid ovals*, *N*-glycosylation. *B*, HEK-293T cells were transfected with the ADAM10 and Tspan15 BiFC expression constructs, fixed, and stained with Alexa Fluor® 647–conjugated Tspan15 mAb 5D4 and analyzed by confocal microscopy. The image shown is representative of middle plane sections taken from two independent experiments (*scale bar*, 10 μm). *C* and *D*, FCS measurements from the upper membrane of HEK-293T expressing the ADAM10/Tspan15 BiFC complexes were used to determine the average particle concentration (*C*) and diffusion coefficient (*D*) of the complexes. *E*, fluorescence fluctuations from the FCS reads were also subjected to PCH analysis to obtain the average molecular brightness (ε) of particles within the confocal volume. The FCS data were separated into groups that preferentially fit to a one-component or a two-component PCH model with dimmer and brighter subcomponents. Data were obtained from 43 individual measurements from three independent experiments. *Error bars*, S.E.; *N*, number of particles; *cpm*, counts per molecule. Data were log-transformed and statistically analyzed by a one-way ANOVA followed by Tukey's multiple-comparison test (***, $p < 0.001$).

ding to a level comparable with that of ADAM10 and Tspan15 transfected as individual constructs, in terms of both basal shedding and shedding induced by the ADAM10 activator NEM (Fig. 9*Ei*). Betacellulin shedding was partially dependent on Tspan15, because ADAM10 transfection alone was not sufficient to fully restore shedding (Fig. 9*Ei*). To confirm expression of the constructs used in these experiments, ADAM10 flow cytometry was used; the fusion protein was expressed at ~2-fold greater levels than ADAM10 individually with Tspan15 (Fig. 9*Eii*). These fusion protein data provide further evidence that ADAM10/Tspan15 exists as a functional scissor complex, because expression and function of the fusion protein are similar to when ADAM10 and Tspan15 are individually co-expressed.

Discussion

This study reports the generation of the first mAbs to tetraspanin Tspan15, which is one of six TspanC8 tetraspanins that regulate the molecular scissor ADAM10 (10, 27, 28) and was recently shown to promote cancer (21). These mAbs enabled five major findings: 1) Tspan15 and ADAM10 co-localize on the cell surface; 2) ADAM10 is the principal Tspan15-interacting protein; 3) Tspan15 expression requires ADAM10; 4) a synthetic ADAM10/Tspan15 fusion protein is a functional scissor; and 5) two of the mAbs have inhibitory activity toward ADAM10/Tspan15. These data strongly suggest that ADAM10 and Tspan15 exist as a heterodimeric scissor complex.

The discovery that Tspan15 expression requires ADAM10 provides genetic evidence that the principal role of Tspan15 is to regulate ADAM10. This finding is consistent with a recent study on Tspan5 and ADAM10 (15). In that study, an approximate 70% siRNA knockdown of ADAM10 in the HCT116 and U2OS cell lines reduced Tspan5 expression by 40%, and ADAM10 was shown to be important for trafficking of Tspan5 out of the ER (15). Our findings are also consistent with a very recent study showing that Tspan15 surface expression is reduced by 60% in ADAM10-knockout PC3 prostate cancer cells (29). In the current study, we investigated Tspan15 expression in the absence of ADAM10 by CRISPR/Cas9 knockout in three different cell lines, namely A549, HEK-293T, and Jurkat. In each ADAM10-knockout cell line, Tspan15 expression was reduced by ~80%, as measured by flow cytometry and Western blotting. Primary HUVECs yielded similar data, because 85–90% ADAM10 knockdown resulted in an equivalent reduction in Tspan15 protein expression. Importantly, Tspan15 mRNA expression levels were unaffected by ADAM10 knockout, indicating a specific effect on Tspan15 protein. Lysosomal inhibition partially restored Tspan15 protein expression, suggesting its instability in the absence of ADAM10, but the latter was still required for Tspan15 cell surface expression. Thus, Tspan15 and ADAM10 appear to be each required for the normal expression of the other. Indeed, it is well-established that TspanC8s are important for ADAM10 maturation and trafficking to the cell surface (6–8, 11–14, 16, 30–33), and we extended these observations by showing that ADAM10 surface expression was partially reduced in the absence of Tspan15 in A549, HEK-293T, and HUVECs. Expression of other TspanC8s by these cells (7, 27) is likely to be the reason that the reduction is only partial. However, the effect of Tspan15 on ADAM10

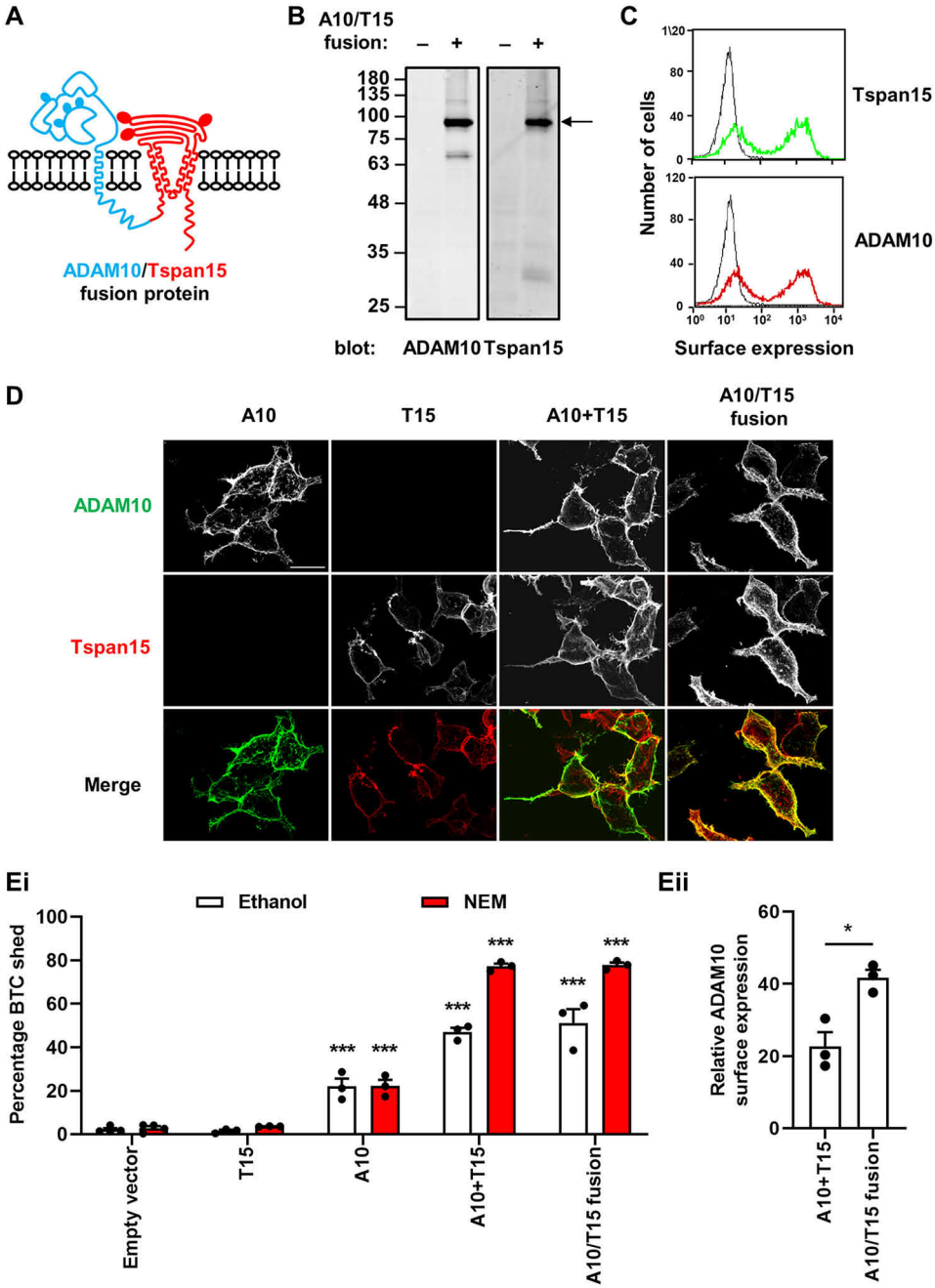

Figure 9. A synthetic ADAM10/Tspan15 fusion protein is a functional scissor. *A*, *schematic representation* of the synthetic ADAM10/Tspan15 fusion protein that has the C terminus of ADAM10 physically linked to the N terminus of Tspan15. *Solid ovals*, *N*-glycosylation. *B*, ADAM10/Tspan15 double-KO HEK-293T cells were transfected with the ADAM10/Tspan15 fusion construct, lysed in 1% digitonin lysis buffer in the presence of 10 μM ADAM10 inhibitor GI254023X, to prevent post-lysis autoproteolysis, and Western blotted for ADAM10 and Tspan15. *C*, cells described in *B* were assessed for surface expression of Tspan15 (*green*) and ADAM10 (*red*) by flow cytometry. *Black traces* represent isotype control staining. *D*, ADAM10/Tspan15 double-KO HEK-293T cells were transfected with the indicated expression constructs and analyzed by confocal microscopy using anti-ADAM10 (*green*) and Tspan15 (*red*) mAbs. The cells were nonpermeabilized, and images are maximum intensity projections of confocal z-stacks. *Scale bar* (*top left image*), 30 μm. *Ei*, ADAM10/Tspan15 double-KO HEK-293T cells were co-transfected with alkaline phosphatase–tagged betacellulin (*BTC*) and Tspan15, ADAM10, ADAM10 and Tspan15, the ADAM10/Tspan15 fusion, or an empty vector control. Cells were stimulated with 2 mM NEM or vehicle control, and alkaline phosphatase activity was measured in the supernatant and whole-cell lysates to quantitate the percentage of BTC shed. Data were arcsine-transformed and statistically analyzed with a two-way ANOVA followed by Tukey's multiple-comparison test (***, $p < 0.001$ compared with empty vector-transfected control). *Eii*, transfected cells were assessed for surface expression of ADAM10 by flow cytometry, and the data were quantitated and analyzed using a paired *t* test (*, $p < 0.05$).

expression is cell type–dependent, because no ADAM10 reduction was observed in Tspan15-knockout Jurkat T cells. It remains unclear why this is the case, but it is possible that Tspan15 protein expression is low in these cells, relative to other tetraspanins.

The previously discussed finding that Tspan15 expression requires ADAM10 suggests that the two proteins might exist as a functional complex. Indeed, we showed for the first time that endogenous Tspan15 and ADAM10 co-localize on the cell surface, using TIRF microscopy, which agrees with a previous

study that used transfected epitope-tagged Tspan15 (6). A prediction of the idea that ADAM10/Tspan15 exist as an intimate complex is that physically linking the two proteins into a single fusion protein would yield a functional scissor protein. Indeed, we found that an ADAM10/Tspan15 fusion protein was expressed at the cell surface at the predicted molecular weight and was functional in a betacellulin shedding assay in a manner that was comparable with when the two proteins were expressed individually. In this shedding assay in the HEK-293T cell line, betacellulin shedding was entirely dependent on ADAM10, as was previously reported in MEFs (26). Our ADAM10/Tspan15 fusion protein is the first example of physically linking a tetraspanin to its partner protein, as a means of demonstrating that the two proteins can function as a complex. This approach may be useful for the investigation of other tetraspanins and their partners. Moreover, it may facilitate attempts to generate the first high-resolution structure of a tetraspanin/partner protein complex, which could provide fundamental new insights comparable with the recently reported first crystal structure of a tetraspanin (5). To date, the only structural study on a tetraspanin with its partner is the relatively low-resolution (6 Å) cryo-EM study of tetraspanin uroplakins Ia and Ib with their uroplakin partners II and IIIa (34).

Our study represents the first use of BiFC to enable the fluorescent imaging of a tetraspanin with its partner. BiFC uses two fusion proteins containing each half of a fluorescent protein, such as GFP, linked to the two proteins of interest, in this case ADAM10 and Tspan15. If the two proteins interact, the two halves of GFP will fold to form a fluorescent GFP molecule, and therefore any fluorescent signal can only be the result of a successful ADAM10/Tspan15 heterodimer. Consistent with the idea that ADAM10 and Tspan15 exist as a functional complex, ADAM10/Tspan15 BiFC dimers were formed and localized predominantly to the plasma membrane, similar to the localization of Tspan15 itself. To investigate the dynamics of ADAM10/Tspan15 dimers for the first time in living cells, FCS was used to investigate its diffusion speed and clustering in the plasma membrane of transfected HEK-293T cells. An average diffusion co-efficient of 0.19 $\mu m^2/s$ was similar to that previously reported for ADAM10 (0.10 $\mu m^2/s$) on Tspan15-transfected U2OS cells (12). However, that study measured ADAM10 rather than ADAM10/Tspan15 dimers (12); therefore, a proportion of the diffusion speed will have been contributed by other ADAM10/TspanC8 complexes. We also used FCS to assess the molecular brightness of ADAM10/Tspan15 BiFC dimers, to estimate the degree of clustering. The existence of some traces containing a brighter Tspan15/ADAM10 component was indicative of larger cluster formation, as has been observed for TspanC8s and other tetraspanins by superresolution microscopy (35–37). We propose that FCS imaging of BiFC dimers will be useful for the study of other tetraspanin/partner protein complexes.

One prediction of the idea that ADAM10 and Tspan15 exist as a heterodimeric complex is that ADAM10 would be the major Tspan15-interacting partner. Using MS to identify proteins in Tspan15 immunoprecipitates from HEK-293T cells lysed in the relatively stringent 1% digitonin, ADAM10 was strikingly the most abundant protein. Indeed, ADAM10 was almost 400 times more abundant in Tspan15 immunoprecipitates from WT cells *versus* control Tspan15-knockout cells, and the only other protein identified above the false discovery rate threshold was Tspan15 itself. It is worth noting that Tspan15-knockout cells are not the perfect negative control for ADAM10 detection in this experiment, because ADAM10 expression is reduced by 60% in these cells. Hence, in Fig. 5, the 400-fold ADAM10 enrichment in the WT cells may be a slight overestimation. These data are consistent with two previous studies in which GFP-tagged Tspan15 was expressed in U2OS or HepG2 cells, which were lysed in relatively nonstringent 1% Brij97 and Tspan15 immunoprecipitated via the GFP tag (12, 20). For example, MS identified ADAM10 as 15-fold more abundant than any other Tspan15-interacting proteins (12). However, interpretation was complicated in these two studies because of the use of less stringent detergent and the resulting large number of tetraspanin-associated proteins identified, the majority of which are likely to be indirectly associated with Tspan15. In our study, in addition to ADAM10, 26 proteins were identified as being significantly more detected in WT *versus* Tspan15-knockout samples, but the most differential of these was only 4-fold higher in WT. Thus, it remains to be determined whether any of these are definitive ADAM10/Tspan15-interacting proteins that impact functionally on the complex. Of note, we did not identify β-transducin repeat–containing E3 ubiquitin protein ligase (BTRC) among the putative Tspan15-interacting proteins. BTRC was recently reported to co-immunoprecipitate with Tspan15 from lysates of esophageal squamous cell carcinoma cell lines and was implicated in promotion of metastasis by Tspan15 via the NF-κB pathway (21). The Human Protein Atlas (RRID:SCR_006710) indicates that BTRC mRNA has a broad expression profile in cell lines, including HEK-293T (17), suggesting that we should have identified BTRC if it is a *bona fide* Tspan15-interacting protein. The findings of our study lead us to speculate that Tspan15 may be promoting cancer via ADAM10, most likely due to cleaving of specific substrates that enhance the cancer phenotype. Interestingly, gene expression data suggest that Tspan15 is strongly up-regulated in cholangiocarcinoma and pancreatic adenocarcinoma (38) and is a marker of poor prognosis in pancreatic, renal, and liver cancer (18). Moreover, Tspan15 has been recently implicated in oral squamous cell carcinoma (19) and hepatocellular carcinoma (20).

The generation of mAbs to certain tetraspanins is a recognized difficulty in the tetraspanin field; there are no mAbs to many of the 33 human tetraspanins. To initiate this study, we generated the first Tspan15 mAbs using a novel strategy. Mice were immunized with ADAM10-knockout MEFs stably overexpressing human Tspan15, with the aim of focusing the mAb response on Tspan15 and preventing the larger ADAM10 from masking epitopes or preventing mAb binding by steric hindrance. Screening of hybridomas yielded four mouse anti-human Tspan15 mAbs, each recognizing a similar epitope on the large extracellular loop of Tspan15. However, the importance of using ADAM10-knockout cells as the immunogen remains unclear. The immunization and hybridoma generation was outsourced to Abpro, whose proprietary mouse may have con-

tributed to the success of our approach. Furthermore, Tspan15 may be a relatively easy target, because eight of the 121 amino acids in the large extracellular loop are different between humans and mice, yielding 93% identity and the likelihood of distinct epitopes for mAb recognition. Most other TspanC8s are more conserved between humans and mice, with identities of 100, 77, 98, 96, and 97% for Tspan5, -10, -14, -17, and -33, respectively. A recent study overcame the problem of the identical human and mouse Tspan5 protein sequences by generating Tspan5 mAbs from Tspan5-knockout mice immunized with GFP-Tspan5–transfected cells and immunoprecipitates (15). Nevertheless, we hypothesize that our new method of using tetraspanin-transfected cells, with the tetraspanin partner(s) deleted, may be an effective strategy for future tetraspanin mAb generation. This hypothesis was supported by our generation of the first five mAbs to human Tspan14. However, these mAbs were only effective in flow cytometry of Tspan14-transfected cells, which is the way the hybridomas were selected, suggesting that they may be low-affinity reagents. Future antibody projects should incorporate procedures that detect endogenous protein to ensure that more effective hybridomas are selected.

Finally, two of our Tspan15 mAbs, clones 1C12 and 4A4, had inhibitory activity toward ADAM10/Tspan15, whereas clones 5D4 and 5F4 did not. This was surprising given that all four mAbs were epitope-mapped to an FSV amino acid sequence within the variable region of the large extracellular loop. A structural model of Tspan15 suggested that these FSV residues are located near the top of the molecule, adjacent to a single α-helix within the variable region. It is possible that subtle differences in epitope or affinity might explain the inhibitory effects of 1C12 and 4A4; interestingly, these mAbs showed comparable binding to overexpressed human and mouse Tspan15 by flow cytometry, whereas 5D4 and 5F4 had significantly reduced binding to mouse. The biological relevance of the inhibitory activities of 1C12 and 4A4 toward ADAM10/Tspan15 is not clear from our relatively simple cell line model. Nevertheless, our data are comparable with the previously reported inhibitory activity of a Tspan5 mAb toward ADAM10/Tspan5 in Notch activation (15). TspanC8 mAbs therefore have potential as therapeutics to treat human diseases promoted by ADAM10.

To conclude, our findings strongly suggest that Tspan15 exists as an ADAM10/Tspan15 scissor complex, which may be a general theme for the other five TspanC8s. We therefore propose that ADAM10 be studied in the context of its associated TspanC8. This has implications for future work that should aim to determine how ADAM10/TspanC8 complexes are triggered to cleave specific substrates and whether ADAM10/TspanC8 complexes can be therapeutically targeted to treat human disease.

Experimental procedures

Antibodies

Primary antibodies were rabbit anti-FLAG (Sigma–Aldrich, Poole, UK), mouse or rabbit anti-α-tubulin (Cell Signaling Technology, London, UK), mouse anti-human ADAM10 11G2 (39), mouse anti-Tspan5 TS52 (15), negative control mouse IgG1 MOPC-21 (MP Biomedicals, Santa Ana, CA), rabbit anti-VE-cadherin D87F2 (Cell Signaling Technology), and mouse anti-human CD9 1AA2 (40).

Expression constructs

pLVX-EF1α-IRES-Puro FLAG-tagged human Tspan15 was generated by subcloning the FLAG-Tspan15 sequence into the pLVX-EF1α-IRES-Puro lentiviral plasmid (Clontech, Mountain View, CA). N-terminal FLAG-tagged human and mouse TspanC8s in the pEF6-*myc*-His plasmid (Invitrogen) were as described (7). A series of human/mouse Tspan15 chimeric constructs were generated using a two-step PCR method to incorporate mouse residues into the human Tspan15 large extracellular loop and vice versa. GFP-tagged human Tspan5/Tspan15 chimeras in the pEGFP-N1 plasmid were as described (15). Human Tspan15 tagged at the C terminus with the N-terminal half of superfolder GFP was generated by subcloning human Tspan15 into a pcDNA3.1/zeo split superfolder GFP vector (41). Mouse ADAM10 tagged at the C terminus with the C-terminal half of superfolder GFP was generated using a two-step PCR approach in which the GFP tag was subcloned into pcDNA3.1 mouse ADAM10 (42). pRK5M human ADAM10 was a gift from Rik Derynck (Addgene plasmid 31717) (43). The pRK5M ADAM10-Tspan15 fusion construct was generated by subcloning human Tspan15 into pRK5M human ADAM10, at the C terminus of ADAM10, to replace the Myc tag. The alkaline phosphatase–tagged human betacellulin construct was kindly provided by Shigeki Higashiyama and Carl Blobel (26). pWPI-human VE-cadherin was generated by PCR of VE-cadherin from HUVEC cDNA, followed by subcloning into pWPI. The pWPI plasmid was a gift from Didier Trono (Addgene plasmid 12254).

Cell culture and transfections

ADAM10-knockout MEFs (23), HEK-293T (HEK-293 cells expressing the large T-antigen of simian virus 40), and the human lung epithelial cell line A549 were cultured in Dulbecco's modified Eagle's medium (Sigma–Aldrich), and the human T cell line Jurkat was cultured in RPMI 1640 (Sigma–Aldrich), each supplemented with 10% fetal bovine serum (Thermo Fisher Scientific, Loughborough, UK), 4 mM L-glutamine, 100 units/ml penicillin, and 100 μg/ml streptomycin (Sigma-Aldrich). HUVECs were isolated from umbilical cords obtained with consent from the Human Biomaterials Resource Centre at the University of Birmingham and cultured in M199 supplemented with 10% fetal bovine serum, 4 mM glutamine, 90 μg/ml heparin (Sigma–Aldrich), and bovine brain extract (44) and used between passages 3 and 6. HEK-293T cells were transfected using polyethyleneimine as described (45). A549 cells were transfected with Lipofectamine 2000 (Thermo Fisher Scientific). Jurkat cells were transfected by electroporation as described previously (46). For siRNA knockdowns, HUVECs were transfected with 10 nM Silencer Select siRNA duplexes (Thermo Fisher Scientific) using Lipofectamine RNAiMAX (Thermo Fisher Scientific).

Generation of CRISPR/Cas9-knockout cell lines

Two guide RNA sequences were selected for each of human ADAM10 and Tspan15 using the Wellcome Trust Sanger Institute's CRISPR Finder tool (47). The following primer pairs were used to encode these sequences: ADAM10 guide 1 (5′-CACCGCGTCTAGATTTCCATGCCCA-3′ and 5′-AAACTGGGCATGGAAATCTAGACGC-3′); ADAM10 guide 2 (5′-CACCGATACCTCTCATATTTACAC-3′ and 5′-AAACGTGTAAATATGAGAGGTATC-3′); Tspan15 guide 1 (5′-CACCGGCGCGCGCTTCTCCTACCTC-3′ and 5′-AAACGAGGTAGGAGAAGCGCGCGCC-3′); Tspan15 guide 2 (5′-CACCGAGCGCCCAGGATGCCGCGCG-3′ and 5′-AAACCGCGCGGCATCCTGGGCGCTC-3′). Each primer pair was annealed and cloned into the pSpCas9 (BB)-2A-Puro (PX459) plasmid (a gift from Feng Zhang, Addgene plasmid 62988) (48). Cells were transfected with either of the guide constructs; clonal transfectants were selected using 1, 2.5, and 0.5 μg/ml puromycin (Thermo Fisher Scientific) for A549, HEK-293T, and Jurkat cells, respectively; and knockouts were confirmed by flow cytometry.

Human platelet preparation

Washed human platelets were isolated from whole-blood by centrifugation as described previously (49). Blood samples were taken with consent from healthy donors.

Generation of new Tspan15 and Tspan14 mAbs

To create the immunogens for mouse anti-human Tspan15 and Tspan14 mAb generation, ADAM10-knockout MEFs were transduced with lentivirus packaged with FLAG-tagged human Tspan15 or Tspan14, produced in HEK-293T cells using a previously described protocol (50). Clonal cells stably overexpressing Tspan15 or Tspan14 were selected with 1 μg/ml puromycin and validated by anti-FLAG Western blotting. Immunization of mice and generation of hybridomas were outsourced to Abpro Therapeutics (Boston, MA).

Antibody conjugation

Purified Tspan15 mAbs were concentrated to 1 mg/ml using Amicon Ultra centrifugal filters (Merck, Watford, UK) and conjugated to Alexa Fluor® 647 fluorophore with a succinimidyl ester–reactive dye (Thermo Fisher Scientific) at an antibody/dye mass ratio of 10:1 for 1 h at room temperature. Excess unbound dye was removed using Zeba Spin desalting columns (Thermo Fisher Scientific). The concentration and degree of labeling of the conjugated mAbs were measured spectrophotometrically.

Flow cytometry

2.5–5 $\times$ 10^5 cells were stained with primary antibodies at 10 μg/ml, followed by FITC-conjugated sheep anti-mouse (Sigma–Aldrich) or allophycocyanin-conjugated goat anti-mouse (Thermo Fisher Scientific) secondary antibodies. Samples were analyzed on a FACSCalibur flow cytometer (BD Biosciences, Oxford, UK). Surface staining was quantitated by its geometric mean fluorescence intensity and presented as a ratio to the isotype control.

Antibody-binding competition assay

A549 cells were incubated with 10 μg/ml MOPC-21 or Tspan15 mAb 1C12, 4A4, 5D4, or 5F4 for 30 min on ice. The cells were then stained with 10 μg/ml of each of the Alexa Fluor® 647–conjugated Tspan15 mAbs for 30 min on ice. Relative antibody binding was analyzed by flow cytometry.

Immunoprecipitation and Western blotting

Immunoprecipitation and Western blotting were performed as described previously (13). Western blotting used IRDye 680RD- or 800CW-conjugated secondary antibodies (LI-COR Biosciences, Cambridge, UK) and an Odyssey Quantitative IR imaging system (LI-COR Biosciences).

Protein structure prediction and computational modeling

The structure of human Tspan15 (UniProt accession number O95858) was predicted and modeled using Phyre2 (51) under intensive mode and visualized with PyMOL. The model generated yielded 100% confidence for 78% of the total protein length, based on the crystal structure of human CD81 (Protein Data Bank code 5TCX) (5). In particular, residues 16–190 and 209–261 were built with 100% confidence, whereas the remainder of the residues, primarily located on the loops, were built *ab initio*, corresponding to lower-confidence regions.

Sample preparation for MS

2 $\times$ 10^8 WT or Tspan15-knockout HEK-293T cells were lysed in 1% digitonin lysis buffer containing protease inhibitor mixture (Sigma-Aldrich). Lysates were precleared with protein G–Sepharose prior to immunoprecipitation with Tspan15 mAb 1C12 chemically cross-linked to protein G–Sepharose with dimethyl pimelimidate (Thermo Fisher Scientific). Five independent immunoprecipitations were carried out for each cell type. Immunoprecipitation samples in nonreducing Laemmli buffer were subjected to a modified single-pot solid phase–enhanced sample preparation (SP3) protocol (52). Briefly, 10 μl of a 4 μg/μl bead slurry of Sera-Mag SpeedBeads A and B (GE Healthcare) were added to the samples. Protein binding to the magnetic beads was achieved by adding acetonitrile to a final volume of 70% (v/v) and mixing at 1200 rpm at 24 °C for 30 min in a Thermomixer (Eppendorf, Hamburg, Germany). Magnetic beads were retained in a DynaMag-2 magnetic rack (Thermo Fisher Scientific), and the supernatant was discarded. Disulfide bridges were reduced by adding 20 μl of 30 mM DTT (Biozol, Eching, Germany) and incubating at 1200 rpm at 37 °C for 30 min. Cysteines were alkylated by adding 25 μl of 80 mM iodoactemamide (Sigma-Aldrich) and incubating at 1200 rpm at 24 °C for 30 min in the dark in a Thermomixer. The reaction was quenched by adding 3 μl of 200 mM DTT. Protein binding to the beads was repeated in 70% (v/v) acetonitrile for 30 min. After removing the solvent, beads were washed twice in 200 μl of 70% (v/v) ethanol and twice in 180 μl of 100% (v/v) acetonitrile. Next, 250 ng of LysC and 250 ng of trypsin (Promega, Mannheim, Germany) were added in 20 μl of 50 mM ammonium bicarbonate (Sigma–Aldrich). The protein digestion was performed for 16 h at room temperature. Samples were acidi-

fied with formic acid to a final concentration of 1% (v/v) and placed in a magnetic rack. The supernatants were transferred into fresh 0.5-ml protein LoBind tubes (Eppendorf). A volume of 20 μl of 2% (v/v) DMSO was added to the beads and subjected to sonication for 30 s in a water bath. Tubes were placed in the magnetic rack, and the supernatants were transferred. The samples were dried in a vacuum centrifuge and dissolved in 20 μl of 0.1% formic acid.

Liquid chromatography coupled with tandem MS (LC-MS/MS) analysis

Samples were analyzed by LC-MS/MS for relative label-free protein quantification. A volume of 10 μl/sample was separated on a nano-LC system (EASY-nLC 1200, Thermo Fisher Scientific) using an in-house packed C18 column (30 cm $\times$ 75-μm inner diameter, ReproSil-Pur 120 C18-AQ, 1.9 μm; Dr. Maisch GmbH, Ammerbuch, Germany) with a binary gradient of water (A) and acetonitrile (B) containing 0.1% formic acid at 50 °C column temperature and a flow rate of 250 nl/min (gradient: 0 min, 2.4% B; 2 min, 4.8% B; 92 min, 24% B; 112 min, 35.2% B; 121 min, 60% B).

The nano-LC was coupled online via a nanospray flex ion source (Proxeon, Thermo Fisher Scientific) equipped with a PRSO-V2 column oven (Sonation, Biberach an der Riss, Germany) to a Q-Exactive HF mass spectrometer (Thermo Fisher Scientific). Full MS spectra were acquired at a resolution of 120,000. The top 15 peptide ions were chosen for higher-energy C-trap dissociation (normalized collision energy of 26%, automatic gain control 1E+5 ions, intensity threshold 5E+3 ions, maximum ion-trapping time 100 ms). Fragment ion spectra were acquired at a resolution of 15,000. A dynamic exclusion of 120 s was used for peptide fragmentation.

Data analysis and label-free quantification

The raw data were analyzed by Maxquant software (Max-Planck Institute Munich) version 1.6.6.0 (53). The MS data were searched against a fasta database of *Homo sapiens* from UniProt (download: June 12, 2019; 20,962 entries). Trypsin was defined as the protease. Two missed cleavages were allowed for the database search. The option first search was used to recalibrate the peptide masses within a window of 20 ppm. For the main search, peptide and peptide fragment mass tolerances were set to 4.5 and 20 ppm, respectively. Carbamidomethylation of cysteine was defined as static modification. Acetylation of the protein N terminus and oxidation of methionine were set as variable modifications. The false discovery rate for both peptides and proteins was adjusted to less than 1%. Label-free quantification of proteins required at least two ratio counts of unique peptides. Only unique peptides were used for quantification. The option "match between runs" was enabled with a matching time of 1 min. The protein label-free quantification intensities were $\log_2$-transformed, and a two-sided Student's t test was applied to evaluate the significance of proteins with changed abundance between the TSPAN15 immunoprecipitation from WT samples and the control immunoprecipitation from Tspan15-knockout samples. Additionally, a permutation-based false discovery rate estimation was used (54). The MS data have been deposited to the ProteomeXchange Consortium via the PRIDE partner repository (55) with the data set identifier PXD016508.

qRT-PCR

RNA was extracted using the RNeasy Mini kit (Qiagen, Manchester, UK) from cells homogenized with QIAshredder columns (Qiagen). Complementary DNA was generated using the High Capacity cDNA Reverse Transcription kit (Thermo Fisher Scientific) and subjected to TaqMan quantitative PCR assays (Thermo Fisher Scientific) for Tspan15 (Hs00202548_m1) and GAPDH (Hs02758991_g1) and analyzed as described (14). All quantitative PCR data were normalized to GAPDH as the internal loading control.

Confocal microscopy

All reagents were from Sigma–Aldrich unless otherwise stated. Cells were fixed with 10% formalin for 15 min and washed three times with PBS (0.01 M phosphate, 0.0027 M KCl, 0.137 M NaCl, pH 7.4) before blocking in PBS containing 1% BSA, 2% goat serum (or mouse serum for direct staining with conjugated mouse primary antibodies), and 0.1% saponin for 20 min to permeabilize the cells. The same buffer was used for antibody dilutions. Cells were incubated with antibodies for 1 h and washed 3–4 times with PBS after incubations. For direct labeling of Tspan15, cells were stained with 5 μg/ml Alexa Fluor® 647–conjugated Tspan15 mAb (5D4). For simultaneous staining of ADAM10 and Tspan15, cells were first stained with 0.5 μg/ml ADAM10 mAb (11G2) and then secondarily labeled with Alexa Fluor®-conjugated goat anti-mouse antibody, followed by direct staining of Tspan15 as described above. Confocal z-stacks of stained cells were taken at 1-μm intervals on a Leica TCS SP2 confocal microscope (Leica Biosystems, Wetzlar, Germany) with 488-nm argon and 633-nm helium/neon laser lines with a $\times$63, 1.4 NA oil objective. For imaging of nonpermeabilized cells, the Nikon A1R confocal system (Nikon, Tokyo, Japan), equipped with a $\times$100, 1.4 NA oil objective and lasers similar to those above, was used for acquisition of z-stacks.

Total internal reflection (TIRF) microscopy

Cells were fixed and stained with 5 μg/ml Tspan15 mAb 5D4 or 1.8 μg/ml CD9 mAb and secondarily labeled with Alexa Fluor®-conjugated goat anti-mouse antibody, followed by direct staining of ADAM10 using 1 μg/ml Alexa Fluor® 647–conjugated ADAM10 mAb. TIRF images of the basal cell membranes were captured sequentially with 488- and 640-nm laser lines with a $\times$100, 1.49 NA oil objective on a Nikon N-STORM microscope. To analyze the degree of co-localization between ADAM10 and Tspan15 or CD9, the images were preprocessed by median filtering and background subtraction to remove noise and subjected to Otsu thresholding (56) before calculating Manders' coefficients (57, 58). All analyses were done using Fiji software (59).

Fluorescence correlation spectroscopy

1.5×10^4 HEK-293T cells were seeded onto Nunc Lab-Tek 8-well glass-bottomed chamber slides (0.13–0.17-mm-thick, #1.0 borosilicate glass) (Thermo Fisher Scientific) precoated

with 10 μg/ml poly-D-lysine (Sigma–Aldrich). 24 h later, cells were transfected with ADAM10 and Tspan15 split sfGFP expression constructs. After a further 24 h, medium was replaced with 200 μl/well HEPES-buffered saline solution (2 mM sodium pyruvate, 145 mM NaCl, 10 mM D-glucose, 5 mM KCl, 1 mM $MgSO_4 \cdot 7H_2O$, 10 mM HEPES, 1.3 mM $CaCl_2$, 1.5 mM $NaHCO_3$, pH 7.45) and equilibrated for 10 min at 22 °C prior to FCS recording on a Zeiss LSM 510NLO ConfoCor 3 microscope (Carl Zeiss, Jena, Germany). Fluorescence fluctuations were collected using a c-Apochromat ×40, 1.2 NA water immersion objective using 488-nm excitation with emission collected through a 505–600 long pass filter. FCS acquisition, autocorrelation, and PCH analyses were performed as described previously (60). In brief, the confocal volume was calibrated with 20 nM rhodamine 6G dye on each experimental day. For cell measurements, the detection volume was positioned in *x-y* over the cell of interest using a live confocal image and then on the apical cell membrane following a *z*-intensity scan using ~0.04 kW/cm^2 laser power. Fluctuation traces were recorded at 22 °C on the apical membrane for each cell for 30 s using ~0.17 kW/cm^2 laser power. Autocorrelation and PCH analyses were performed in Zen 2012 (Carl Zeiss), with the first 5 s of fluctuations routinely removed to adjust for photobleaching. Autocorrelation curves were fitted to a two-component, two-dimensional diffusion model with a pre-exponential term to account for sfGFP blinking, with an offset added where necessary to obtain average dwell times and particle numbers. As previously demonstrated, component 1 (300–600 μs) represents a dark state of the sfGFP fluorophore, whereas component 2 represents the dwell time of the sfGFP-labeled complex (41, 60). Diffusion coefficients of the sfGFP-labeled complex were calculated for each trace using the equation, $D = \omega_0^2/4.\tau_D$, where ω_0 is the radius of the detection volume (obtained from calibration) and τ_D is the average dwell time of component 2. Particle numbers of component 2 were expressed as particles/μm^2, calculated from $n = N(\tau_{D2})/\pi \cdot \omega_0^2$, where $N(\tau_{D2})$ is the fractional contribution of component 2 to the total particle number determined from the autocorrelation curve. Molecular brightness of complexes was determined using PCH analyses carried out on the same fluctuation traces as used for autocorrelation analyses using Zen 2012. Traces were binned at 100 μs and fitted to either a one- or two-component PCH model with the first-order correction fixed at 0.3, as determined from the calibration read. Data are shown as values obtained from individual cell membranes, obtained over *n* independent transfections.

VE-cadherin cleavage assay

HEK-293T cells were transfected with a VE-cadherin expression construct. Cells were treated with 10 μM DAPT (Sigma-Aldrich) to prevent post-ADAM10 proteolysis by γ-secretase, followed by 2 mM NEM (Sigma-Aldrich) for 30 min to activate ADAM10. Cells were lysed in 1% Triton X-100 lysis buffer and subjected to Western blotting with an antibody against the cytoplasmic tail of VE-cadherin.

Betacellulin shedding assay

ADAM10/Tspan15 double-knockout HEK-293T cells were transfected in 24-well plates with 200 ng of alkaline phosphatase–conjugated betacellulin expression construct and 50 ng total of ADAM10, Tspan15, ADAM10 plus Tspan15, or the ADAM10/Tspan15 fusion construct. 24 h post-transfection, cells were washed and stimulated with 2 mM NEM or ethanol vehicle control for 2.5 h in Opti-MEM reduced serum medium (Thermo Fisher Scientific). Alkaline phosphatase activity in supernatant and cell lysate samples was measured using *p*-nitrophenyl phosphate substrate (Sigma–Aldrich) and a VICTOR X3 multilabel plate reader (PerkinElmer, Seer Green, UK). The supernatant activity as a percentage of the total was calculated to determine the percentage shedding.

Statistical analyses

Relative data were normalized by either log or arscine transformation before being statistically analyzed using ANOVA with post hoc multiple-comparison tests, as indicated in the figure legends.

Author contributions—C. Z. K., N. H., P. J. N., H.-E. H., S. A. M., J. G., A. D. M., S. F. L., and M. G. T. data curation; C. Z. K., N. H., P. J. N., J. S., A. L. M., H.-E. H., S. A. M., J. T., J. G., K. W., A. D. M., S. F. L., and M. G. T. formal analysis; C. Z. K. and N. H. validation; C. Z. K., N. H., P. J. N., J. S., A. L. M., H.-E. H., S. A. M., J. T., J. G., K. W., C. A., B. C., E. D., M. K., A. M., T. A. M., P. R. M., H. T. H. N., M. C. S., H. A., A. D. M., L. S., and C. P. investigation; C. Z. K. and N. H. writing-original draft; H.-E. H., S. A. M., J. T., J. G., A. D. M., N. S. P., S. J. B., N. D. H., and S. F. L. methodology; H.-E. H., S. A. M., J. G., P. S., E. R., S. J. B., N. D. H., and M. G. T. writing-review and editing; P. S., E. C., N. S. P., S. F. L., and M. G. T. supervision; E. R. resources; N. S. P., S. J. B., N. D. H., and M. G. T. funding acquisition; M. G. T. conceptualization; M. G. T. project administration.

Acknowledgments—We are grateful to Jeremy Pike for help with TIRF microscopy image analysis and to members of the Cells and Molecules research theme in the School of Biosciences for helpful comments on this project. We thank Stefan Düsterhöft, Andreas Ludwig, and Carol Murphy for useful discussions and Neil Barclay and Andrew McKnight for advice on antibody generation. We also thank the Birmingham Advanced Light Microscope Facility and COMPARE for advice on fluorescence microscopy.

References

1. Lichtenthaler, S. F., Lemberg, M. K., and Fluhrer, R. (2018) Proteolytic ectodomain shedding of membrane proteins in mammals-hardware, concepts, and recent developments. *EMBO J.* **37,** CrossRef Medline
2. Wetzel, S., Seipold, L., and Saftig, P. (2017) The metalloproteinase ADAM10: a useful therapeutic target? *Biochim. Biophys. Acta Mol. Cell Res.* **1864,** 2071–2081 CrossRef Medline
3. Termini, C. M., and Gillette, J. M. (2017) Tetraspanins function as regulators of cellular signaling. *Front. Cell Dev. Biol.* **5,** 34 CrossRef Medline
4. van Deventer, S. J., Dunlock, V. E., and van Spriel, A. B. (2017) Molecular interactions shaping the tetraspanin web. *Biochem. Soc. Trans.* **45,** 741–750 CrossRef Medline
5. Zimmerman, B., Kelly, B., McMillan, B. J., Seegar, T. C. M., Dror, R. O., Kruse, A. C., and Blacklow, S. C. (2016) Crystal structure of a full-length human tetraspanin reveals a cholesterol-binding pocket. *Cell* **167,** 1041–1051.e11 CrossRef Medline

6. Dornier, E., Coumailleau, F., Ottavi, J. F., Moretti, J., Boucheix, C., Mauduit, P., Schweisguth, F., and Rubinstein, E. (2012) TspanC8 tetraspanins regulate ADAM10/Kuzbanian trafficking and promote Notch activation in flies and mammals. *J. Cell Biol.* **199,** 481–496 CrossRef Medline
7. Haining, E. J., Yang, J., Bailey, R. L., Khan, K., Collier, R., Tsai, S., Watson, S. P., Frampton, J., Garcia, P., and Tomlinson, M. G. (2012) The TspanC8 subgroup of tetraspanins interacts with A disintegrin and metalloprotease 10 (ADAM10) and regulates its maturation and cell surface expression. *J. Biol. Chem.* **287,** 39753–39765 CrossRef Medline
8. Prox, J., Willenbrock, M., Weber, S., Lehmann, T., Schmidt-Arras, D., Schwanbeck, R., Saftig, P., and Schwake, M. (2012) Tetraspanin15 regulates cellular trafficking and activity of the ectodomain sheddase ADAM10. *Cell Mol. Life Sci.* **69,** 2919–2932 CrossRef Medline
9. Matthews, A. L., Koo, C. Z., Szyroka, J., Harrison, N., Kanhere, A., and Tomlinson, M. G. (2018) Regulation of leukocytes by TspanC8 tetraspanins and the "molecular scissor" ADAM10. *Front. Immunol.* **9,** 1451 CrossRef Medline
10. Matthews, A. L., Noy, P. J., Reyat, J. S., and Tomlinson, M. G. (2017) Regulation of A disintegrin and metalloproteinase (ADAM) family sheddases ADAM10 and ADAM17: the emerging role of tetraspanins and rhomboids. *Platelets* **28,** 333–341 CrossRef Medline
11. Brummer, T., Müller, S. A., Pan-Montojo, F., Yoshida, F., Fellgiebel, A., Tomita, T., Endres, K., and Lichtenthaler, S. F. (2019) NrCAM is a marker for substrate-selective activation of ADAM10 in Alzheimer's disease. *EMBO Mol. Med.* **11,** e9695 CrossRef Medline
12. Jouannet, S., Saint-Pol, J., Fernandez, L., Nguyen, V., Charrin, S., Boucheix, C., Brou, C., Milhiet, P. E., and Rubinstein, E. (2016) TspanC8 tetraspanins differentially regulate the cleavage of ADAM10 substrates, Notch activation and ADAM10 membrane compartmentalization. *Cell Mol. Life Sci.* **73,** 1895–1915 CrossRef Medline
13. Noy, P. J., Yang, J., Reyat, J. S., Matthews, A. L., Charlton, A. E., Furmston, J., Rogers, D. A., Rainger, G. E., and Tomlinson, M. G. (2016) TspanC8 tetraspanins and a disintegrin and metalloprotease 10 (ADAM10) interact via their extracellular regions: evidence for distinct binding mechanisms for different TspanC8 proteins. *J. Biol. Chem.* **291,** 3145–3157 CrossRef Medline
14. Reyat, J. S., Chimen, M., Noy, P. J., Szyroka, J., Rainger, G. E., and Tomlinson, M. G. (2017) ADAM10-interacting tetraspanins Tspan5 and Tspan17 regulate VE-cadherin expression and promote T lymphocyte transmigration. *J. Immunol.* **199,** 666–676 CrossRef Medline
15. Saint-Pol, J., Billard, M., Dornier, E., Eschenbrenner, E., Danglot, L., Boucheix, C., Charrin, S., and Rubinstein, E. (2017) New insights into the tetraspanin Tspan5 using novel monoclonal antibodies. *J. Biol. Chem.* **292,** 9551–9566 CrossRef Medline
16. Seipold, L., Altmeppen, H., Koudelka, T., Tholey, A., Kasparek, P., Sedlacek, R., Schweizer, M., Bär, J., Mikhaylova, M., Glatzel, M., and Saftig, P. (2018) *In vivo* regulation of the A disintegrin and metalloproteinase 10 (ADAM10) by the tetraspanin 15. *Cell Mol. Life Sci.* **75,** 3251–3267 CrossRef Medline
17. Thul, P. J., Åkesson, L., Wiking, M., Mahdessian, D., Geladaki, A., Ait Blal, H., Alm, T., Asplund, A., Björk, L., Breckels, L. M., Bäckström, A., Danielsson, F., Fagerberg, L., Fall, J., Gatto, L., *et al.* (2017) A subcellular map of the human proteome. *Science* **356,** eaal3321 CrossRef Medline
18. Uhlen, M., Zhang, C., Lee, S., Sjöstedt, E., Fagerberg, L., Bidkhori, G., Benfeitas, R., Arif, M., Liu, Z., Edfors, F., Sanli, K., von Feilitzen, K., Oksvold, P., Lundberg, E., Hober, S., *et al.* (2017) A pathology atlas of the human cancer transcriptome. *Science* **357,** eaan2507 CrossRef Medline
19. Hiroshima, K., Shiiba, M., Oka, N., Hayashi, F., Ishida, S., Fukushima, R., Koike, K., Iyoda, M., Nakashima, D., Tanzawa, H., and Uzawa, K. (2019) Tspan15 plays a crucial role in metastasis in oral squamous cell carcinoma. *Exp. Cell Res.* **384,** 111622 CrossRef Medline
20. Sidahmed-Adrar, N., Ottavi, J. F., Benzoubir, N., Ait Saadi, T., Bou Saleh, M., Mauduit, P., Guettier, C., Desterke, C., and Le Naour, F. (2019) Tspan15 is a new stemness-related marker in hepatocellular carcinoma. *Proteomics* **19,** e1900025 CrossRef Medline
21. Zhang, B., Zhang, Z., Li, L., Qin, Y. R., Liu, H., Jiang, C., Zeng, T. T., Li, M. Q., Xie, D., Li, Y., Guan, X. Y., and Zhu, Y. H. (2018) TSPAN15 interacts with BTRC to promote oesophageal squamous cell carcinoma metastasis via activating NF-κB signaling. *Nat. Commun.* **9,** 1423 CrossRef Medline
22. Rubinstein, E., Charrin, S., and Tomlinson, M. G. (2013) Organisation of the tetraspanin web. in *Tetraspanins* (Berditchevski, F., and Rubinstein, E., eds) pp. 47–90, Springer, Dordrecht, Netherlands
23. Reiss, K., Maretzky, T., Ludwig, A., Tousseyn, T., de Strooper, B., Hartmann, D., and Saftig, P. (2005) ADAM10 cleavage of N-cadherin and regulation of cell-cell adhesion and β-catenin nuclear signalling. *EMBO J.* **24,** 742–752 CrossRef Medline
24. Tomlinson, M. G., Hanke, T., Hughes, D. A., Barclay, A. N., Scholl, E., Hünig, T., and Wright, M. D. (1995) Characterization of mouse CD53: epitope mapping, cellular distribution and induction by T cell receptor engagement during repertoire selection. *Eur. J. Immunol.* **25,** 2201–2205 CrossRef Medline
25. Tomlinson, M. G., Williams, A. F., and Wright, M. D. (1993) Epitope mapping of anti-rat CD53 monoclonal antibodies. Implications for the membrane orientation of the transmembrane 4 superfamily. *Eur. J. Immunol.* **23,** 136–140 CrossRef Medline
26. Sahin, U., Weskamp, G., Kelly, K., Zhou, H. M., Higashiyama, S., Peschon, J., Hartmann, D., Saftig, P., and Blobel, C. P. (2004) Distinct roles for ADAM10 and ADAM17 in ectodomain shedding of six EGFR ligands. *J. Cell Biol.* **164,** 769–779 CrossRef Medline
27. Matthews, A. L., Szyroka, J., Collier, R., Noy, P. J., and Tomlinson, M. G. (2017) Scissor sisters: regulation of ADAM10 by the TspanC8 tetraspanins. *Biochem. Soc. Trans.* **45,** 719–730 CrossRef Medline
28. Saint-Pol, J., Eschenbrenner, E., Dornier, E., Boucheix, C., Charrin, S., and Rubinstein, E. (2017) Regulation of the trafficking and the function of the metalloprotease ADAM10 by tetraspanins. *Biochem. Soc. Trans.* **45,** 937–944 CrossRef Medline
29. Eschenbrenner, E., Jouannet, S., Clay, D., Chaker, J., Boucheix, C., Brou, C., Tomlinson, M. G., Charrin, S., and Rubinstein, E. (2020) TspanC8 tetraspanins differentially regulate ADAM10 endocytosis and half-life. *Life Sci. Alliance* **3,** e201900444 CrossRef Medline
30. Brummer, T., Pigoni, M., Rossello, A., Wang, H., Noy, P. J., Tomlinson, M. G., Blobel, C. P., and Lichtenthaler, S. F. (2018) The metalloprotease ADAM10 (a disintegrin and metalloprotease 10) undergoes rapid, postlysis autocatalytic degradation. *FASEB J.* **32,** 3560–3573 CrossRef Medline
31. Shah, J., Rouaud, F., Guerrera, D., Vasileva, E., Popov, L. M., Kelley, W. L., Rubinstein, E., Carette, J. E., Amieva, M. R., and Citi, S. (2018) A dock-and-lock mechanism clusters ADAM10 at cell-cell junctions to promote α-toxin cytotoxicity. *Cell Rep.* **25,** 2132–2147.e7 CrossRef Medline
32. Virreira Winter, S., Zychlinsky, A., and Bardoel, B. W. (2016) Genome-wide CRISPR screen reveals novel host factors required for *Staphylococcus aureus* α-hemolysin-mediated toxicity. *Sci. Rep.* **6,** 24242 CrossRef Medline
33. Zhou, J., Fujiwara, T., Ye, S., Li, X., and Zhao, H. (2014) Downregulation of Notch modulators, tetraspanin 5 and 10, inhibits osteoclastogenesis *in vitro*. *Calcif. Tissue Int.* **95,** 209–217 CrossRef Medline
34. Min, G., Wang, H., Sun, T. T., and Kong, X. P. (2006) Structural basis for tetraspanin functions as revealed by the cryo-EM structure of uroplakin complexes at 6-Å resolution. *J. Cell Biol.* **173,** 975–983 CrossRef Medline
35. Dahmane, S., Doucet, C., Le Gall, A., Chamontin, C., Dosset, P., Murcy, F., Fernandez, L., Salas, D., Rubinstein, E., Mougel, M., Nollmann, M., and Milhiet, P. E. (2019) Nanoscale organization of tetraspanins during HIV-1 budding by correlative dSTORM/AFM. *Nanoscale* **11,** 6036–6044 CrossRef Medline
36. Marjon, K. D., Termini, C. M., Karlen, K. L., Saito-Reis, C., Soria, C. E., Lidke, K. A., and Gillette, J. M. (2016) Tetraspanin CD82 regulates bone marrow homing of acute myeloid leukemia by modulating the molecular organization of N-cadherin. *Oncogene* **35,** 4132–4140 CrossRef Medline
37. Zuidscherwoude, M., Göttfert, F., Dunlock, V. M., Figdor, C. G., van den Bogaart, G., and van Spriel, A. B. (2015) The tetraspanin web revisited by super-resolution microscopy. *Sci. Rep.* **5,** 12201 CrossRef Medline
38. Tang, Z., Kang, B., Li, C., Chen, T., and Zhang, Z. (2019) GEPIA2: an enhanced web server for large-scale expression profiling and interactive analysis. *Nucleic Acids Res.* **47,** W556–W560 CrossRef Medline
39. Arduise, C., Abache, T., Li, L., Billard, M., Chabanon, A., Ludwig, A., Mauduit, P., Boucheix, C., Rubinstein, E., and Le Naour, F. (2008) Tetras-

panins regulate ADAM10-mediated cleavage of TNF-α and epidermal growth factor. *J. Immunol.* **181,** 7002–7013 CrossRef Medline
40. Sincock, P. M., Mayrhofer, G., and Ashman, L. K. (1997) Localization of the transmembrane 4 superfamily (TM4SF) member PETA-3 (CD151) in normal human tissues: comparison with CD9, CD63, and $\alpha5\beta1$ integrin. *J. Histochem. Cytochem.* **45,** 515–525 CrossRef Medline
41. Kilpatrick, L. E., Briddon, S. J., and Holliday, N. D. (2012) Fluorescence correlation spectroscopy, combined with bimolecular fluorescence complementation, reveals the effects of β-arrestin complexes and endocytic targeting on the membrane mobility of neuropeptide Y receptors. *Biochim. Biophys. Acta* **1823,** 1068–1081 CrossRef Medline
42. Maretzky, T., Schulte, M., Ludwig, A., Rose-John, S., Blobel, C., Hartmann, D., Altevogt, P., Saftig, P., and Reiss, K. (2005) L1 is sequentially processed by two differently activated metalloproteases and presenilin/γ-secretase and regulates neural cell adhesion, cell migration, and neurite outgrowth. *Mol. Cell. Biol.* **25,** 9040–9053 CrossRef Medline
43. Liu, C., Xu, P., Lamouille, S., Xu, J., and Derynck, R. (2009) TACE-mediated ectodomain shedding of the type I TGF-beta receptor downregulates TGF-β signaling. *Mol. Cell* **35,** 26–36 CrossRef Medline
44. Wilson, E., Leszczynska, K., Poulter, N. S., Edelmann, F., Salisbury, V. A., Noy, P. J., Bacon, A., Rappoport, J. Z., Heath, J. K., Bicknell, R., and Heath, V. L. (2014) RhoJ interacts with the GIT-PIX complex and regulates focal adhesion disassembly. *J. Cell Sci.* **127,** 3039–3051 CrossRef Medline
45. Ehrhardt, C., Schmolke, M., Matzke, A., Knoblauch, A., Will, C., Wixler, V., and Ludwig, S. (2006) Polyethylenimine, a cost-effective transfection reagent. *Signal Transduct.* **6,** 179–184 CrossRef
46. Tomlinson, M. G., Calaminus, S. D., Berlanga, O., Auger, J. M., Bori-Sanz, T., Meyaard, L., and Watson, S. P. (2007) Collagen promotes sustained glycoprotein VI signaling in platelets and cell lines. *J. Thromb. Haemost.* **5,** 2274–2283 CrossRef Medline
47. Hodgkins, A., Farne, A., Perera, S., Grego, T., Parry-Smith, D. J., Skarnes, W. C., and Iyer, V. (2015) WGE: a CRISPR database for genome engineering. *Bioinformatics* **31,** 3078–3080 CrossRef Medline
48. Ran, F. A., Hsu, P. D., Wright, J., Agarwala, V., Scott, D. A., and Zhang, F. (2013) Genome engineering using the CRISPR-Cas9 system. *Nat. Protoc.* **8,** 2281–2308 CrossRef Medline
49. McCarty, O. J., Calaminus, S. D., Berndt, M. C., Machesky, L. M., and Watson, S. P. (2006) von Willebrand factor mediates platelet spreading through glycoprotein Ib and α(IIb)β3 in the presence of botrocetin and ristocetin, respectively. *J. Thromb. Haemost.* **4,** 1367–1378 CrossRef Medline
50. Reyat, J. S., Tomlinson, M. G., and Noy, P. J. (2017) Utilizing lentiviral gene transfer in primary endothelial cells to assess lymphocyte-endothelial interactions. *Methods Mol. Biol.* **1591,** 155–168 CrossRef Medline
51. Kelley, L. A., Mezulis, S., Yates, C. M., Wass, M. N., and Sternberg, M. J. (2015) The Phyre2 web portal for protein modeling, prediction and analysis. *Nat. Protoc.* **10,** 845–858 CrossRef Medline
52. Hughes, C. S., Moggridge, S., Müller, T., Sorensen, P. H., Morin, G. B., and Krijgsveld, J. (2019) Single-pot, solid-phase-enhanced sample preparation for proteomics experiments. *Nat. Protoc.* **14,** 68–85 CrossRef Medline
53. Cox, J., Hein, M. Y., Luber, C. A., Paron, I., Nagaraj, N., and Mann, M. (2014) Accurate proteome-wide label-free quantification by delayed normalization and maximal peptide ratio extraction, termed MaxLFQ. *Mol. Cell. Proteomics* **13,** 2513–2526 CrossRef Medline
54. Tusher, V. G., Tibshirani, R., and Chu, G. (2001) Significance analysis of microarrays applied to the ionizing radiation response. *Proc. Natl. Acad. Sci. U.S.A.* **98,** 5116–5121 CrossRef Medline
55. Perez-Riverol, Y., Csordas, A., Bai, J., Bernal-Llinares, M., Hewapathirana, S., Kundu, D. J., Inuganti, A., Griss, J., Mayer, G., Eisenacher, M., Pérez, E., Uszkoreit, J., Pfeuffer, J., Sachsenberg, T., Yilmaz, S., *et al.* (2019) The PRIDE database and related tools and resources in 2019: improving support for quantification data. *Nucleic Acids Res.* **47,** D442–D450 CrossRef Medline
56. Otsu, N. (1979) A threshold selection method from gray-level histograms. *IEEE Trans. Syst. Man Cybern.* **9**, 62–66 CrossRef
57. Manders, E. M. M., Verbeek, F. J., and Aten, J. A. (1993) Measurement of colocalization of objects in dual-color confocal images. *J. Microsc.* **169,** 375–382 CrossRef
58. Pike, J. A., Styles, I. B., Rappoport, J. Z., and Heath, J. K. (2017) Quantifying receptor trafficking and colocalization with confocal microscopy. *Methods* **115,** 42–54 CrossRef Medline
59. Schindelin, J., Arganda-Carreras, I., Frise, E., Kaynig, V., Longair, M., Pietzsch, T., Preibisch, S., Rueden, C., Saalfeld, S., Schmid, B., Tinevez, J. Y., White, D. J., Hartenstein, V., Eliceiri, K., Tomancak, P., and Cardona, A. (2012) Fiji: an open-source platform for biological-image analysis. *Nat. Methods* **9,** 676–682 CrossRef Medline
60. Ayling, L. J., Briddon, S. J., Halls, M. L., Hammond, G. R., Vaca, L., Pacheco, J., Hill, S. J., and Cooper, D. M. (2012) Adenylyl cyclase AC8 directly controls its micro-environment by recruiting the actin cytoskeleton in a cholesterol-rich milieu. *J. Cell Sci.* **125,** 869–886 CrossRef Medline
61. Sievers, F., Wilm, A., Dineen, D., Gibson, T. J., Karplus, K., Li, W., Lopez, R., McWilliam, H., Remmert, M., Söding, J., Thompson, J. D., and Higgins, D. G. (2011) Fast, scalable generation of high-quality protein multiple sequence alignments using Clustal Omega. *Mol. Syst. Biol.* **7,** 539 CrossRef Medline